

Repurposing of a Nucleoside Scaffold from Adenosine Receptor Agonists to Opioid Receptor Antagonists

Dilip K. Tosh,^{†,‡} Antonella Ciancetta,^{†,‡,#} Philip Mannes,[†] Eugene Warnick,[†] Aaron Janowsky,[‡] Amy J. Eshleman,[‡] Elizabeth Gizewski,[§] Tarsis F. Brust,^{||} Laura M. Bohn,^{||} John A. Auchampach,[§] Zhan-Guo Gao,[†] and Kenneth A. Jacobson^{*,†,§}

[†]Molecular Recognition Section, Laboratory of Bioorganic Chemistry, National Institute of Diabetes and Digestive and Kidney Diseases, National Institutes of Health, 9000 Rockville Pike, Bethesda, Maryland 20892, United States

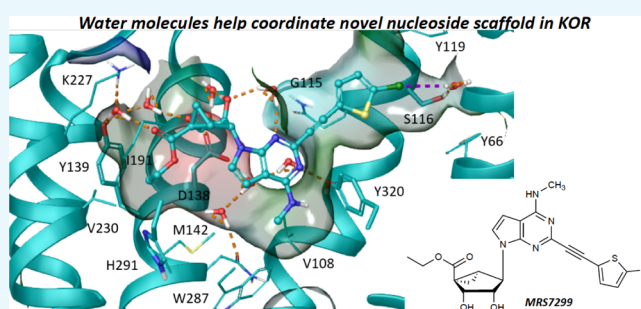
[‡]VA Portland Health Care System, Research Service (R&D-22), and Departments of Psychiatry and Behavioral Neuroscience, Oregon Health and Science University, 3710 S.W. U.S. Veterans Hospital Blvd., Portland, Oregon 97239, United States

[§]Department of Pharmacology, Medical College of Wisconsin, 8701 Watertown Plank Road, Milwaukee, Wisconsin 53226, United States

^{||}Departments of Molecular Medicine and Neuroscience, The Scripps Research Institute, 130 Scripps Way, Jupiter, Florida 33458, United States

Supporting Information

ABSTRACT: While screening off-target effects of rigid (*N*)-methanocarba-adenosine 5'-methylamides as A₃ adenosine receptor (AR) agonists, we discovered μ M binding hits at the δ -opioid receptor (DOR) and translocator protein (TSPO). In an effort to increase OR and decrease AR affinity by structure activity analysis of this series, antagonist activity at κ -(K)OR appeared in 5'-esters (ethyl **24** and propyl **30**), which retained TSPO interaction (μ M). 7-Deaza modification of C2-(arylethynyl)-5'-esters but not 4'-truncation enhanced KOR affinity (MRS7299 **28** and **29**, $K_i \approx 40$ nM), revealed μ -OR and DOR binding, and reduced AR affinity. Molecular docking and dynamics simulations located a putative KOR binding mode consistent with the observed affinities, placing C7 in a hydrophobic region. 3-Deaza modification permitted TSPO but not OR binding, and 1-deaza was permissive to both; ribose-restored analogues were inactive at both. Thus, we have repurposed a known AR nucleoside scaffold for OR antagonism, with a detailed hypothesis for KOR recognition.



INTRODUCTION

Nucleoside analogues containing a bicyclo[3.1.0]hexane ring system (termed methanocarba, Chart 1) in place of ribose are being developed as highly selective A₃ adenosine receptor (AR) agonists, which have potential in treatment of chronic neuropathic pain and other conditions.^{1,2} The position of cyclopropyl and cyclopentyl ring fusion enforces a South (S) or a North (N) envelope conformation, which we previously showed to promote A₃AR interaction.^{2,3} This rigid scaffold shows promise as a privileged but not promiscuous structural class for interaction with diverse protein targets.⁴ Varied off-target effects of these nucleosides at biogenic amine receptors, including as SHT_{2B} and SHT_{2C} serotonin receptor antagonists, and as allosteric modulators of the dopamine transporter (DAT), were detected at higher concentrations than their nM affinities at the A₃AR. Moreover, it was possible to enhance these novel activities, while at the same time deselecting for AR affinity.^{5,6}

We report here that certain (*N*)-methanocarba nucleosides can also antagonize opioid receptors (ORs): δ - (DOR), κ -

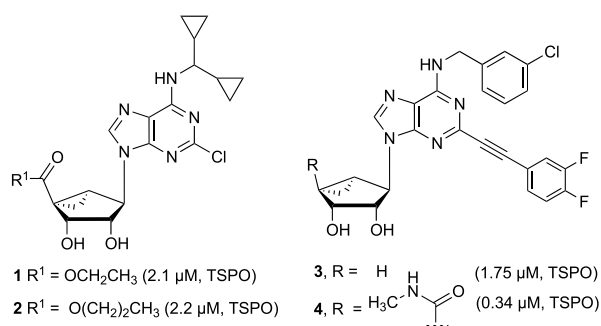
(KOR), and μ - (MOR), with moderate preference for KOR. We probed the structure–activity relationship (SAR) of rigid bicyclic nucleosides to enhance KOR affinity and modeled their receptor interactions. We have also proposed a structural basis for the unexpected interaction of rigid nucleosides with the KOR, especially 7-deaza analogues,^{7,8} utilizing modeling approaches that complement published reports on KOR modeling.^{9–11} We also observed a partial SAR convergence with the translocator protein (TSPO), but this was not the target of the present study. The affinity at TSPO and DOR was noted previously for a few (*N*)-methanocarba adenosine derivatives.⁴ For example, the *N*⁶-dicyclopropylmethyl 5'-ester derivatives **1** and **2** displayed roughly μ M affinity at TSPO, while also binding to A₁AR and A₃AR.⁵ Other rigid bicyclic nucleosides, **3** and **4**, with enlarged substituents at the

Received: June 4, 2018

Accepted: September 19, 2018

Published: October 4, 2018

Chart 1. Rigid (N)-Methanocarba Nucleosides with Reported Off-Target Activity at rTSPO^{24a}



^aAll three nucleosides lack significant binding affinity at the hKOR. N⁶-(3-Chlorobenzyl) derivative 4 also activates the human (h) A₃AR ($K_i = 3$ nM), and corresponding 4'-truncated derivative 3 is an A₃AR antagonist ($K_i = 100$ nM).

N⁶ and C2 positions were shown to bind at TSPO as well, and compound 4 also bound weakly at DOR.⁴

High-affinity antagonists of KOR have been reported, including both morphinans and non-morphinans.^{10,12–15} Centrally active KOR antagonists, including those containing novel scaffolds and having shorter half-lives in vivo, are sought for the treatment of mood disorders, drug addiction, pain, and depression resulting from chronic stress.^{16,17} KOR activation by the native peptide dynorphin in the amygdala inhibits presynaptic glutamate release, and its deletion or blockade with selective antagonists produces an anxiolytic phenotype.¹⁸ KOR activation impeded lung cancer cell growth through activation of glycogen synthase kinase 3 β .¹⁹ MOR antagonists may be applied to addiction treatment and to reducing side effects of opioid pain killers when their action is peripherally restricted.^{20–22} TSPO, an off-target interaction of many of nucleosides in this chemical series, is a component of the permeability transition pore on the outer mitochondrial membrane in microglial and other cells, and its ligands provide neuroprotective and anticancer properties.^{23–29} Structurally diverse TSPO ligands are being explored for treatment of chronic pain, inflammation, anxiety, mood disorders, neurodegeneration, and diseases of cellular proliferation.^{30,31} Thus, both of these membrane-bound protein families are important therapeutic targets.

RESULTS

Here, we extend the polypharmacology of rigid nucleosides to enhance affinity at KOR by functional group or heterocyclic replacement on the same scaffold, in some cases with accompanying moderate affinity at TSPO. Furthermore, we discovered modifications of the adenine moiety and its substituents that allowed MOR and/or DOR interactions as antagonists. The receptor interactions of representative nucleosides, based on a KOR X-ray crystallographic structure, were modeled to provide a self-consistent hypothesis for recognition. In this study, we did not model the TSPO interaction or probe the effects of the methanocarba ring isomer having the opposite South (S) conformation.³² Thus, we have repurposed a nucleoside scaffold from ARs to bind at another rhodopsin-like G protein-coupled receptor (GPCR) family.^{5,33}

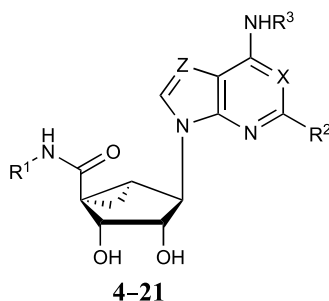
Compound Design. The previously noted binding of (N)-methanocarba nucleosides 1 and 2 at the rat kidney TSPO was

dependent on the presence of a 5'-ethyl or 5'-*n*-propyl ester.⁷ These esters bound to TSPO with greater affinity than the corresponding 5'-methyl ester or 5'-methylamide, which had K_i values >10 μM (data not shown). Removing the alkylloxycarbonyl group of 1, that is, to give an N⁶-dicyclopropylmethyl 4'-truncated analogue (structure not shown), also prevented TSPO binding.⁴ Thus, a medium-sized 5'-alkyl ester was conducive to TSPO interaction. However, with enlarged substituents at both N⁶ and C2 positions, 5'-methylamide 4 bound with greater affinity at the TSPO than 5'-esters 1 and 2 or its 4' truncated equivalent 3. Thus, we explored here the interplay between the 5', N⁶ and C2 positions and adenine ring nitrogens in the SAR of rigid nucleosides initially at TSPO and subsequently at the ORs.

The current study began with a focus on N⁶-3-chlorobenzyl 5'-methylamide derivatives (Table 1, 4–9), but that scope was subsequently expanded to include a range of other N⁶-alkyl or N⁶-alkylaryl derivatives with 5'-carbonyl groups (Tables 2 and 3, 10–43). To explore the SAR around the detected OR and TSPO interactions of nucleosides, we chose to modify the rigid adenosine derivatives at the 5' position, from amides to esters, and at the N⁶ and C2 positions. The default C2 substitution was 5-chloro-thien-2-yl-ethynyl, upon which halogen was substituted, or other arylolethynyl groups were introduced. We included various 4'-truncated (Tables 4 and 5, 47–58) and other derivatives that were synthesized previously in the context of ARs or DAT.^{2,3,5,6,34,35} In addition, N⁶-propyl (19 and 20) and 1-, 3-, or 7-deaza-adenine (17, 26–29, 39–44 and 54–58) analogues were prepared for this study.

Chemical Synthesis. We previously reported the synthesis of numerous 5'-methylamide and 5'-ester derivatives (and truncated derivatives) of N⁶-alkyl C2-arylalkynyl (N)-methanocarba nucleosides similar to 1–4.^{2,3,6,36,37} The synthesis of analogues with C2–H (17, Scheme S1), N⁶-propyl-modified (19, 20, Scheme S2), and 1-deaza (26, Scheme S3) modifications is described in the Supporting Information.

The synthesis of target 7-deaza-2-arylalkynyl nucleosides began with a C2-iodo derivative 72 of the nucleobase (Scheme 1). Initially, compound 60 (Supporting Information, Scheme S4) was subjected to a lithiation reaction with *n*-BuLi in the presence of Bu₃SnCl. However, instead of the desired product, it gave an unanticipated butyl keto derivative 63, which was further transformed to 2-iodo compound 64. C6 amination of compound 64 with methylamine followed by a Sonogashira coupling with 5-chloro-thienylacetylene and subsequent acid hydrolysis provided the 5'-(butyl-keto) nucleoside 44. To overcome this barrier to the synthesis of 7-deaza nucleosides, a convergent approach was designed. 7-Deaza-6-chloro purine 67 was silylated with TIPSCl in the presence of NaH to yield the protected pyrrolo[2,3-*d*]pyrimidine 68. Stannylation of 68 with Bu₃SnCl in the presence of *n*-BuLi provided the tin derivative 69, which upon treatment with iodine and subsequent silyl deprotection afforded 7-deaza-2-iodo-purine 71. Mitsunobu condensation of 71 with glycosyl donor 59³⁸ gave the nucleoside precursor 72, which was aminated at the 6 position with various amines to provide compounds 73–76 (Scheme 1). Sonogashira coupling of iodo derivatives (73–76) with various alkynes using PdCl₂(Ph₃P)₂ as a catalyst followed by acid hydrolysis of the respective derivatives (77–82) with 10% trifluoroacetic acid (TFA) afforded the final hypermodified nucleosides (28–29, 40–43). Acid hydrolysis of 2-iodo derivative 73 yielded the nucleoside 5'-ester 39.

Table 1. Structures and Modulation of Binding and Activity at hORs, rTSPO and A₃AR of (N)-Methanocarba Adenosine Derivatives (4–21) Containing a 5'-Carbonyl Group; (N)-Methanocarba-5'-amides; X, Z = N and R¹ = CH₃, Unless Noted

compound	R ² =, other changes	R ³ =	DOR, ^{a,b} K _i , nM	TSPO, ^b K _i , nM	DAT, ^b % of control at 10 μM (%)	A ₃ AR binding K _i , nM (species), ^d or % of control at 10 μM
4 ^d	3,4-F ₂ -phenylethynyl	CH ₂ -(3-Cl-Ph)	2480 ± 790	340 ± 72	16	3.49 ± 1.84 (h), 3.08 ± 0.23 (m)
5 ^d	Cl	CH ₂ -(3-Cl-Ph)	^e	^f	3	0.29 ± 0.04 (h)
6	phenyl-ethynyl	CH ₂ -(3-Cl-Ph)	^e	2650 ± 290	7	1.35 ± 0.30 (h)
7 ^d	4-F-phenylethynyl	CH ₂ -(3-Cl-Ph)	6620 ± 1700	253 ± 57	21	2.16 ± 0.34 (h)
8 ^d	2-Cl-phenylethynyl	CH ₂ -(3-Cl-Ph)	^f	344 ± 149	50	1.92 ± 0.57 (h)
9	3-Cl-phenylethynyl	CH ₂ -(3-Cl-Ph)	5870 ± 2120	1770 ± 910	26	4.45 ± 1.39 (h)
10	phenylethynyl	<i>trans</i> -cPr-Ph	^e	^f	2310 ^c	6.16 ± 0.22 (h)
11 ^d	5-Cl-thienyl-ethynyl	CH ₃	^e	^e	-322	1.65 ± 0.08 (h), 86 ± 6 (m)
12	phenylethynyl	CH ₃	^e	^e	-211	0.85 ± 0.22 (h)
13	2-Cl-phenyl-ethynyl	CH ₃	^e	^e	-484	0.58 ± 0.04 (h), 110 ± 5 (m)
14 ^d	5-Cl-thienyl-ethynyl	CH ₃	^e	684 ± 175	-556	0.70 ± 0.11 (h), 36 ± 5 (m)
15 ^d	5-Br-thienyl-ethynyl	CH ₃	^e	^f	-235	0.44 ± 0.12 (h), 43.7 ± 2.1 (m)
16 ^d	5-Cl-thienyl-ethynyl, X = CH	CH ₃	^e	^e	1	3.0 ± 0.8 (h), 31 ± 2 (m)
17	H, Z = CH	CH ₃	^e	^e	-14	498 ± 46 (h), 38 ± 1% (m)
18 ^d	5-Cl-thienyl-ethynyl	(CH ₂) ₂ CH ₃	^e	1310 ± 210	-159	1.1 ± 0.3 (h), 6.8 ± 0.3 (m)
19	5-Cl-thienyl-ethynyl	(CH ₂) ₂ CF ₃	^e	1300 ± 150	15	3.7 ± 1.0 (h), 71 ± 2 (m)
20	5-Cl-thienyl-ethynyl	(CH ₂) ₃ OH	^e	6160 ± 50	-107 ± 4	2.04 ± 1.46 (h), 105 ± 2 (m)
21 ^a	5-Cl-thienylethynyl, R ¹ = (CH ₂) ₂ NH ₂	CH ₃	^f	>10 000	-136	158 ± 8 (h), 0% (m)

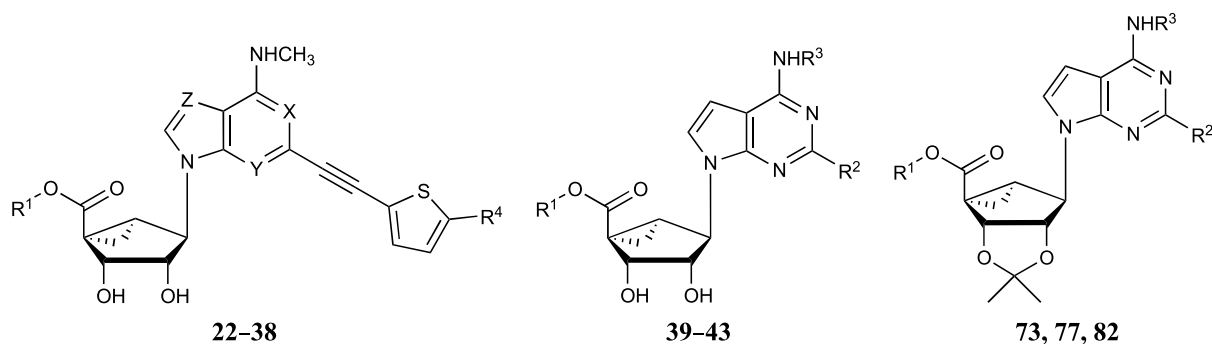
^aKOR and MOR binding inhibition is <50% at 10 μM, unless noted. **21**: KOR, K_i = 2.79 ± 0.77 μM. ^bModulation of inhibition of binding of opioid agonist radioligands [³H]Tyr-D-Ala-Gly-Phe-D-Leu ([³H]DADLE, **97**, 0.2 nM) for DOR, [³H]N-methyl-2-phenyl-N-[(5*R*,7*S*,8*S*)-7-(pyrrolidin-1-yl)-1-oxaspiro[4.5]dec-8-yl]acetamide ([³H]U69593, **98**, 0.3 nM) for KOR, [³H]Ala2-MePhe4-Glyol5-Enkephalin ([³H]DAMGO, **99**, 0.3 nM) for MOR; and [³H]nociceptin **100** (0.5–2.0 nM) for NOP. [³H]N-Butan-2-yl-1-(2-chlorophenyl)-N-methylisoquinoline-3-carboxamide ([³H]PK11195, **101**, 1.0 nM) was used for rat TSPO, and [³H]methyl(1*R*,2*S*,3*S*)-3-(4-fluorophenyl)-8-methyl-8-azabicyclo[3.2.1]octane-2-carboxylate ([³H]WIN35428 **103**, 0.5 nM) was used for DAT. NOP binding K_i values (μM, *n* = 1) were found to be **4** (3.90) and **9** (>10). Reference ligands and their K_i values (nM) were DOR, natrindole **108**, 0.81; KOR, salvinorin A **109**, 1.93; MOR, morphine **110**, 3.29; NOP, 7-[[4-(2,6-dichlorophenyl)-1-piperidinyl]methyl]-6,7,8,9-tetrahydro-1-methyl-5*H*-benzocyclohepten-5-ol (SB612111) **111**, 6.58; TSPO, 4'-chlorodiazepam (Ro5-4864) **112**, 27.6; DAT, 1-[2-[bis-(4-fluorophenyl)methoxy]ethyl]-4-(3-phenylpropyl)piperazine (GBR12909) **114**, 3.04. Values are expressed as the mean ± SEM of *N* = 2–4 assays performed in duplicate, unless indicated. ^cK_i (μM), inhibition of binding of [³H]**103** at hDAT: **10**, 2.31. ^dA₃AR and other AR binding data and procedures from Tosh et al.^{2,3,6,34,35,37} [¹²⁵I]N⁶-(4-Amino-3-iodobenzyl)adenosine-5'-N-methyl-uronamide ([¹²⁵I]AB-MECA, **102**, 0.5 nM) was used for hA₃AR. Reference ligand [adenosine-5'-N-ethyluronamide (NECA, **113**)], and its K_i value (nM) was hA₃AR, 35; mA₃AR, 0.45. Representative binding inhibition at hA₁AR is (% at 10 μM) **7**, 22%; **18**, 22%; **19**, 46%; **26**, 39%; **40**, 35%; **41**, 44%; **42**, 34%; **43**, 26%. Representative binding inhibition at hA_{2A}AR (% at 10 μM): **18**, 34%; **19**, 21%; **26**, 16%; **40**, 22%; **41**, 25%; **42**, 20%; **43**, <10%. K_i values (hA₁AR, nM): **55**, 1300 ± 290; **56**, 650 ± 71; **73**, 1110 ± 470; determined as reported.³⁷ mA₁AR and mA_{2A}AR binding data, % inhibition at 10 μM, respectively: **24**, 43 ± 2, 10 ± 3; **26**, 54 ± 1, 5 ± 1; **28**, 32 ± 2, 10 ± 3; **30**, 53 ± 2, 13 ± 2; **46**, 62 ± 2, 12 ± 4. Values are expressed as the mean ± SEM of *N* = 3 assays performed in duplicate. ^e30–50% inhibition of radioligand binding at 10 μM. ^f<30% inhibition of radioligand binding at 10 μM.

4'-Truncated 7-deaza nucleosides (**54–58**) were synthesized in a similar fashion starting from the truncated pseudosugar **83**³⁹ (Scheme 2). Intermediate **83** was coupled with 7-deaza-2-iodo-purine **71** under Mitsunobu conditions to give the nucleoside derivative **84**, which was aminated with various amines to yield compounds **85–87**. A Sonogashira coupling of compounds **85–87** with various alkynes gave C2-functionalized derivatives **88–91**. Acid hydrolysis of compounds **88** and **89** with 10% TFA afforded final nucleosides **54** and **55**. However, attempted acid hydrolysis of compounds **90** and **91** in the presence of 10% TFA gave complex mixtures

because of the high acid sensitivity of the dicyclopropylmethylamino group;⁷ Dowex 50 was used as an alternative. Thus, isopropylidene deprotection of compound **87** with Dowex 50 followed by a Sonogashira coupling with phenylacetylene or 5-bromo-thien-2-ylacetylene afforded nucleosides **56** and **57**, respectively.

Pharmacological Testing. Assays of ORs and TSPO. Screening of the nucleoside derivatives at the human (h) ORs (Tables 1–5, Figures S1–S3, Supporting Information), including selected analogues at the nociceptin receptor (NOP), and rat kidney TSPO (Figure S4) and at other off-

Table 2. Structures and Modulation of Binding and Activity at hORs, rTSP0 and A₃AR of (N)-Methanocarpa Adenosine Derivatives (22–43) and Iodo Derivative (82) Containing a 5'-Carbonyl Group; (N)-Methanocarpa 5'-Esters and Carboxylate; X, Y and Z = N, R³ = CH₃ and R⁴ = Cl, Unless Noted



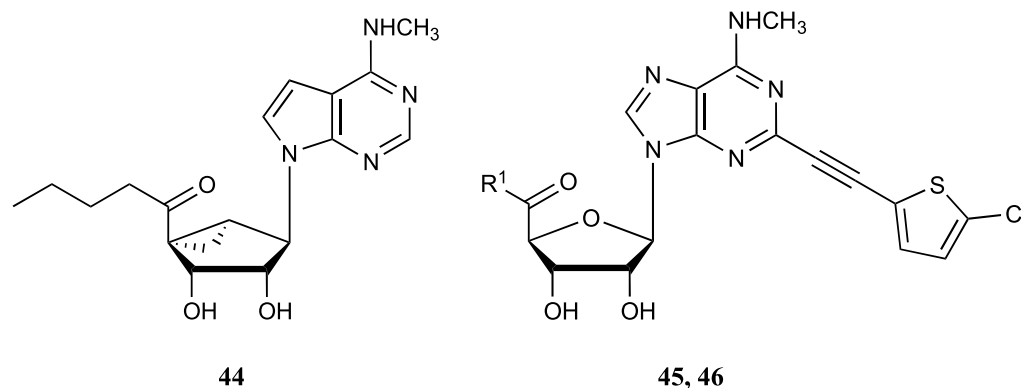
Compound	R ¹ =, other changes	DOR, ^a K _v , nM	KOR, ^a K _v , nM	MOR, ^a K _v , nM	TSP0, ^a K _v , nM	DAT, ^a inhib., % of control at 10 μM, %	A ₃ AR binding K _i , nM (species), ^b or % at 10 μM
22 ^b	CH ₃	^d	3130 ± 300	^c	^c	-352	5.38 ± 0.03 (h), 36 ± 1% (m)
23 ^b	CH ₃ , R ⁴ = Br	^d	2090 ± 330	^c	8120 ± 670	-370	8.56 ± 0.10 (h), 57 ± 1% (m)
24 ^b	CH ₂ CH ₃	^c	396 ± 29	^d	1290 ± 70	-539	14.5 ± 2.3 (h), 45 ± 5% (m)
25	CH ₂ CH ₃ , R ⁴ = Br	^c	975 ± 198	^c	1520 ± 250	-430	6.42 ± 0.35 (h), 1800 ± 90 (m)
26	CH ₂ CH ₃ , X = CH	^c	806 ± 263	^c	3810 ± 100	<10	29.4 ± 13.8 (h), 828 ± 51 (m)
27	CH ₂ CH ₃ , Y = CH	^d	^d	^d	3390 ± 640	-354	47.3 ± 18.9 (h), 18 ± 4% (m)
28	CH ₂ CH ₃ , Z = CH	786 ± 210	42 ± 1	637 ± 367	869 ± 160	-172 ± 57 (3)	448 ± 13 (h), 15 ± 1% (m)
77	CH ₂ CH ₃ , R ² = Cl-thienyl-C≡C	1990 ± 1020	52 ± 23	1530 ± 560	^d	-20	1650 ± 330 (h)
29	CH ₂ CH ₃ , Z = CH, R ⁴ = Br	437 ± 94	39 ± 1	368 ± 135	765 ± 118	-102 ± 8 (3)	466 ± 20 (h), 24 ± 2% (m)
30	(CH ₂) ₂ CH ₃	^d	437 ± 167	^d	1160 ± 560	-426	5.78 ± 1.45 (h), 2810 ± 150 (m)
31	CH(CH ₃) ₂	^d	^d	^d	^d	<20	42.9 ± 22.8 (h), 30 ± 1% (m)
32	(CH ₂) ₃ CH ₃	^d	1210 ± 100	^d	>10 000	-285	17.5 ± 1.6 (h), 54 ± 1% (m)
33	(CH ₂) ₂ -CH(CH ₃) ₂	^d	1090 ± 320	^d	>10 000	-196 ± 58	24.4 ± 2.8 (h), 32 ± 2% (m)
34	(CH ₂) ₂ -cHex	^c	>10 000	^d	^c	<20	334 ± 132 (h), 32 ± 1% (m)
35	CH ₂ -Ph	^d	629 ± 183	^c	4050 ± 740	<20	7.81 ± 2.40 (h), 891 ± 105 (m)
36	(CH ₂) ₂ -Ph	^d	3670 ± 1640	^d	^d	<20	114 ± 64 (h), 31 ± 1% (m)
37	(CH ₂) ₃ -Ph	^d	8920 ± 1080	^d	1090 ± 290	<20	132 ± 68 (h), 40 ± 1% (m)
38	H	^d	^d	^d	^d	-50	684 ± 195 (h), 0% (m)
39	CH ₂ CH ₃ , R ³ = I	1590 ± 280	104 ± 35	^c	^d	<10	390 ± 139 (h)
73	CH ₂ CH ₃ , R ³ = I	>10 000	276 ± 65	7600	>10 000	-39	4050 ± 740 (h)
40	CH ₂ CH ₃ , R ² = phenylethynyl	1780 ± 410	91.5 ± 23.7	1480 ± 450	>10 000	-66	344 ± 40 (h), 15 ± 1% (m)
41	CH ₂ CH ₃ , R ³ = cPr, R ² = phenylethynyl	2400 ± 90	852 ± 137	2110 ± 590	^c	-312	228 ± 115 (h), 41 ± 1% (m)
42	CH ₂ CH ₃ , R ³ = CH ₂ -cPr, R ² = phenylethynyl	^c	1400 ± 210	1300 ± 530	4470 ± 1330	-13	791 ± 433 (h), 30 ± 1% (m)
43	CH ₂ CH ₃ , R ³ = (CH ₂) ₂ Ph, R ² = phenylethynyl	627 ± 178	207 ± 21	1770 ± 540	480 ± 200	21	483 ± 62 (h), 51 ± 1% (m)
82	CH ₂ CH ₃ , R ³ = (CH ₂) ₂ Ph, R ² = phenylethynyl	881 ± 158	217 ± 100	>10 000	>10 000	-24	905 ± 144 (h)

^aBinding assays performed as specified in Table 1, unless noted. NOP binding K_i values (μM, n = 1) were found to be 24 (>10), 25 (9.40), 28 (3.45), 29 (2.09), 35 (>10), and 40 (>10). Values are expressed as the mean ± SEM of N = 2–4 assays performed in duplicate, unless indicated. ^bA₃AR binding data from Tosh et al.^{2,3,6,34,35,37} Representative binding inhibition at hA₁AR is (% at 10 μM) 26, 39%; 40, 35%; 41, 44%; 42, 34%; 43, 26%. Representative binding inhibition at hA_{2A}AR is (% at 10 μM) 26, 16%; 40, 22%; 41, 25%; 42, 20%; 43, <10%; determined as reported.³⁷ mA₁AR and mA_{2A}AR binding data, % inhibition at 10 μM (mean ± SEM, n = 3), respectively: 24, 43 ± 2, 10 ± 3; 26, 54 ± 1, 5 ± 1; 28, 32 ± 2, 10

Table 2. continued

± 3 ; **30**, 53 ± 2 , 13 ± 2 . Values are expressed as the mean \pm SEM of $N = 3$ assays performed in duplicate. ^c30–50% inhibition of radioligand binding at $10 \mu\text{M}$. ^d<30% inhibition of radioligand binding at $10 \mu\text{M}$.

Table 3. Structures and Modulation of Binding and Activity at hORs, rTSPO and A₃AR of (N)-Methanocarba Adenosine Derivatives (44 and 45) and Ribose Derivative (46) Containing a 5'-Carbonyl Group; (N)-Methanocarba-5'-ketone and 9-Riboside Derivatives^a



compound	R ¹ =, other change	KOR, ^b K _i , nM	DAT, ^b inhib., % of control at $10 \mu\text{M}$, %	A ₃ AR binding K _i , nM (species) ^b or % of control at $10 \mu\text{M}$
44		2610 ± 660	-9	98 ± 30 (h), $41 \pm 1\%$ (m)
45^c	NHCH ₃	^e	-321	1.55 ± 0.03 (h), 1170 ± 40 (m)
46^c	OCH ₃	^d	-220	11.5 ± 0.9 (h), 34 ± 2 (m)

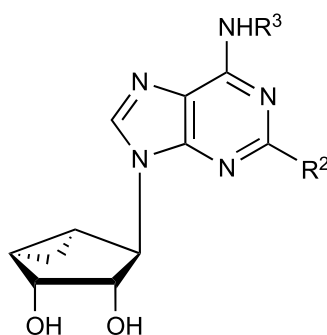
^aDOR, MOR, and TSPO binding inhibition is <50% at $10 \mu\text{M}$. NOP binding K_i value (μM , $n = 1$): **44** (8.65). ^bBinding assays performed as specified in Table 1. Values are expressed as the mean \pm SEM of $N = 2-4$ assays performed in duplicate, unless indicated. ^cA₃AR binding data from Tosh et al.^{2,3,6,34,35,37} Representative binding inhibition at mA₁AR and mA_{2A}AR, % inhibition at $10 \mu\text{M}$, respectively: **46**, 62 ± 2 , 12 ± 4 . Values are expressed as the mean \pm SEM of $N = 3$ assays performed in duplicate. ^d30–50% inhibition of radioligand binding at $10 \mu\text{M}$. ^e<30% inhibition of radioligand binding at $10 \mu\text{M}$.

target sites, was performed by the Psychoactive Drug Screening Program (PDSP). Initially, radioligand binding assays were performed using membranes of mammalian cells overexpressing the receptor of interest.⁴⁰ The following opioid agonist radioligands were used: [³H]Tyr-D-Ala-Gly-Phe-D-Leu ([³H]-DADLE, **97**) for DOR; [³H]*N*-methyl-2-phenyl-*N*-[(5*R*,7*S*,8*S*)-7-(pyrrolidin-1-yl)-1-oxaspiro[4.5]dec-8-yl]-acetamide ([³H]U69593, **98**) for KOR; [³H]Ala²-MePhe⁴-Gly⁵-Enkephalin ([³H]DAMGO, **99**) for MOR; and [³H]-nociceptin **100** for NOP. [³H]*N*-Butan-2-yl-1-(2-chlorophenyl)-*N*-methylisoquinoline-3-carboxamide ([³H]PK11195, **101**) was used for TSPO. Other reagents are found in the Supporting Information. Binding data for three neurotransmitter transporters, that is, DAT, the norepinephrine transporter (NET) and the serotonin transporter (SERT), as well as the A₃AR, using methods previously reported,^{3,33} were also included for comparison. A primary radioligand binding screen was performed at each target protein using a fixed nucleoside concentration of $10 \mu\text{M}$, and those compounds showing >50% inhibition were assayed with full concentration-dependent curves. Binding data determined by PDSP for these compounds at other diverse receptors and channels are described below and detailed in Figure S5 (Supporting Information) and in some cases in previous publications.^{2,5,8} To further explore the potential off-target activities in the (N)-methanocarba nucleoside series, we examined A₃AR agonists **14** and **18** in broad screens of 240 GPCRs and 486 kinases, and there were no additional outstanding interactions at $10 \mu\text{M}$ at any of these sites (Supporting Information). Thus, the specificity for a few interactions was high, and these nucleosides are not promiscuous binders.

3,4-Difluoro 5'-methylamide derivative **4** has been studied as an A₃AR agonist for reducing chronic neuropathic pain, and some of its weak off-target activities, including DOR, were already reported.^{4,36} Compound **4** bound to DOR with a K_i value of $2.48 \pm 0.79 \mu\text{M}$ ($n = 4$), while its 4-fluoro-7 and 3-chloro-phenylethynyl **9** analogues bound more weakly. Substitution of the terminal 3,4-difluorophenyl group of **4** with 2-Cl-Ph **8** prevented binding affinity at DOR, but this and other compounds in this series (**4** and **7**) bound to TSPO with K_i values ~ 300 nM.⁴ Thus, the DOR affinity was sensitive to the C2-terminal aryl group, whereas the TSPO affinity was less sensitive. A *N*⁶-(*trans*-phenyl-cyclopropyl) group in **10** (diastereomeric mixture) was not associated with measurable binding affinity at TSPO or ORs. None of the subsequent 5'-methylamides **11–20** at $10 \mu\text{M}$ significantly inhibited DOR binding (by >50%).

In the series of *N*⁶-methyl 5'-methylamides, a C2-(5-chlorothien-2-yl-ethynyl) **14** but not a 5-bromothien-2-yl-ethynyl **15** group was tolerated in TSPO binding, but only one 5-chlorothien-2-yl-ethynyl derivative in the 5'-methylamide series, **21**, displayed OR binding affinity. Thus, a 5'-amide extension as a 2-aminoethylamide in **21** introduced μM affinity at KOR (K_i $2.9 \mu\text{M}$) while reducing TSPO binding affinity (Figure S2). A 1-deaza substitution of **14** in compound **16** prevented TSPO binding, but its effect on KOR could not be probed in the 5'-amide series, because the reference compound **14** was inactive. *N*⁶-Alkyl extensions to substituted *n*-propyl moieties in **18–20** maintained μM affinity at TSPO with no significant KOR binding.

Unlike 5'-methylamide **14**, the corresponding 5'-methyl ester **22** and its 5-bromothien-2-yl-ethynyl analogue **23** displayed μM affinity at KOR but weaker affinity than **14** at

Table 4. Binding Activity of 4'-Truncated (N)-Methanocarba Derivatives at hORs, hA₃AR and TSPO and Transporters; 4'-Truncated (N)-Methanocarba Adenosine Derivatives**3, 47–53**

compound	R ² =	R ³ =	DOR, ^{a,b} K _i , nM	TSPO, ^b K _i , nM	DAT, ^b inhibition, % of control at 10 μM, %	NET, ^b inhibition, % of control at 10 μM, %	A ₃ AR binding K _i , nM (species) ^{b,e}
3 ^b	3,4-F ₂ -phenyl-ethynyl	CH ₂ -(3-Cl-Ph)	<i>g</i>	1750 ± 360	16	51	100 ± 30 (h)
47	phenyl-ethynyl	CH ₂ -(3-Cl-Ph)	8000 ± 1000	1640 ± 160	37	34	39.0 ± 20.0 (h), 299 ± 3 (m)
48 ^b	H	CH ₂ -(3-Cl-Ph)	<i>g</i>	<i>g</i>	−2	35	4.9 ± 0.7 (h)
49 ^b	phenyl-ethynyl	CH ₃	<i>g</i>	<i>f</i>	−213	<i>c</i>	5.48 ± 1.23 (h), 1530 ± 240 (m)
50 ^b	phenyl-ethynyl	CH ₂ CH ₃	<i>g</i>	<i>f</i>	−154	<i>d</i>	5.02 ± 2.19 (h), 1480 ± 170 (m)
51 ^b	phenyl-ethynyl	(CH ₂) ₂ -Ph	<i>g</i>	<i>g</i>	24	<i>d</i>	20 ± 6 (h), 480 ± 90 (m)
52 ^b	2-Cl-phenyl-ethynyl	(CH ₂) ₂ -Ph	<i>f</i>	877 ± 368	7	24	37.0 ± 7.0 (h)
53 ^b	phenyl-ethynyl	CH ₂ CH-(Ph) ₂	<i>g</i>	3570 ± 1820	17	5780 ^d	200 ± 20 (h)

^aKOR and MOR binding inhibition is <50% at 10 μM. NOP binding K_i for compound 47 was found to be >10 μM. ^bBinding assays performed as specified in Table 1, unless noted. Values are expressed as the mean ± SEM of N = 2–4 assays performed in duplicate, unless indicated. ^c61% inhibition of radioligand binding at 10 μM. ^dK_i (μM), inhibition of binding of [³H]104 at NET: 50, 8.66; 51, 2.8. ^eA₃AR binding data from Toshi et al.^{3,34,35} Representative binding inhibition at hA₁AR is (% at 10 μM) 49, 18%; 50, 36%; 51, 30%; representative binding inhibition at hA_{2A}AR is (% at 10 μM, or K_i) 47, 670 nM; 49, 18%; 50, 42%; 51, 22%; determined as reported.³⁷ Values are expressed as the mean ± SEM of N = 3 assays performed in duplicate. ^f30–50% inhibition of radioligand binding at 10 μM. ^g<30% inhibition of radioligand binding at 10 μM.

TSPO. Furthermore, an increased affinity of homologated 5'-alkyl esters at KOR was revealed, and TSPO affinity of <1 μM was determined (Figure S2). Specifically, the ethyl 24 and *n*-propyl 31 esters displayed K_i values at KOR of ~400 nM. The 5-halo-thiophene substitution in the ethyl ester series indicated an order of affinity of Cl ≥ Br (25) at KOR. The 5'-*i*-propyl ester 31 and the corresponding carboxylic acid 38 were inactive at both KOR and TSPO. Further 5'-ester elongation to *n*-Bu in compound 32 and *i*-pentyl in compound 33 decreased the KOR affinity ~threefold compared with 24 but greatly reduced TSPO affinity. Inclusion of cyclohexyl and phenyl groups on the 5'-ester moiety in 34–37 led to variable moderate (μM) KOR affinity or inactivity, with O-benzyl derivative 35 having the highest affinity (K_i 629 nM).

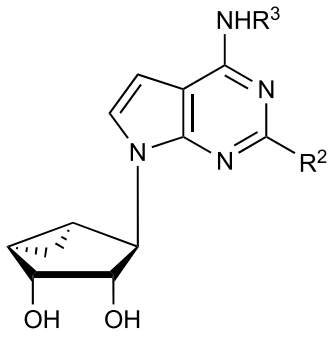
Compound 26 allowed the effects of the 1-deaza modification to be examined in the 5'-ester series, demonstrating small affinity decreases at KOR and TSPO compared with 24. A 3-deaza modification in 27 was permissive for TSPO binding but prevented KOR binding. In contrast to the requirement for the N3 in KOR binding, a 7-deaza modification in esters 28 and 29 both enhanced KOR affinity (~40 nM) and allowed DOR and MOR affinity to appear (Figure S3). The preference for KOR in comparison to DOR and MOR was 19- and 15-fold for 28 and 11- and 9-fold for 29, respectively. The preference for KOR in comparison to TSPO was ~20-fold for both 28 and 29.

In the 7-deaza-5'-ester series, modified N⁶ and C2 substituents were explored. C2-phenylethynyl analogue 40 had 2–3-fold lower affinity at ORs than the corresponding C2-(5-chlorothien-2-yl-ethynyl) analogue 28 and was inactive at TSPO. N⁶-Cyclopropyl 41 and cyclopropylmethyl 42 groups reduced the OR affinity compared with N⁶-methyl 40. N⁶-2-Phenylethyl-substituted analogue 43 was comparable to N⁶-methyl analogue 40 in OR affinity, but with enhanced TSPO affinity (K_i 480 nM). Compound 77, a 2',3'-isopropylidene-protected precursor of 28 had the same binding affinity at KOR, but was weaker in TSPO binding. Compound 82, the isopropylidene-protected precursor of 43, maintained affinity at both DOR and KOR, but not MOR.

The inactivity of the ribose derivatives 45 and 46 compared with their corresponding (N)-methanocarba derivatives 14 and 22, respectively, showed that the rigid (N)-methanocarba ring is required for interaction with both KOR and TSPO. In the methanocarba series, 2-iodo 5'-ethyl ester 39 was included to test the requirement for an extended C2 substituent; in comparison to 28, there was only a ~2-fold affinity decrease at DOR and KOR and a large decrease at MOR and TSPO.

We extended the SAR analysis to a set of 4'-truncated nucleosides in the same methanocarba series (Tables 4 and 5), to determine if a 7-deaza modification was also OR affinity-enhancing without a 5'-ester and to analyze the effects of substitution at N⁶ and C2 positions (Tables 4 and 5, 3, 47–

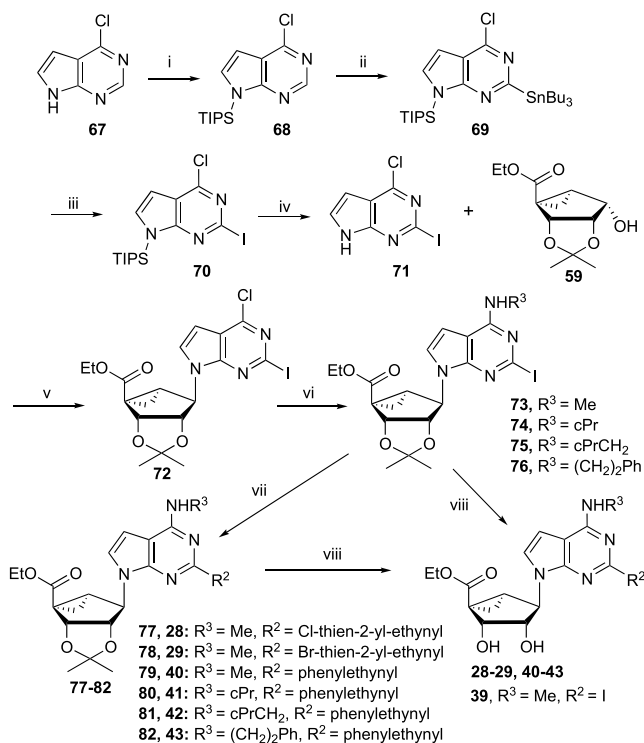
Table 5. Binding Activity of 4'-Truncated (N)-Methanocarpa Derivatives at hORs, hA₃AR and TSPO and Transporters; 4'-Truncated (N)-Methanocarpa 7-Deaza-adenosine Derivatives^a



compound	R ² =	R ³ =	DOR, ^b K _i , nM	KOR, ^b K _i , nM	MOR, ^b K _i , nM	TSPO, ^b K _i , nM	A ₃ AR binding K _i , nM (species), ^c or % of control at 10 μM
54 ^a	phenyl-ethynyl	CH ₃	^d	1120 ± 220	2670 ± 280	^e	85.6 ± 12.0 (h), 11 ± 1% (m)
55 ^a	phenyl-ethynyl	(CH ₂) ₂ -Ph	3660 ± 1330	1370 ± 180	4020 ± 890	2120 ± 230	217 ± 65 (h), 29 ± 2% (m)
56	phenyl-ethynyl	CH(cPr) ₂	2550 ± 660	^d	1440 ± 750	4210 ± 1840	178 ± 32 (h)
57	5-Br-thienyl-ethynyl	CH(cPr) ₂	>10 000	3020 ± 90	>10 000	>10 000	2440 ± 430 (h)
58	I	CH(cPr) ₂	^e	^e	^e	^e	5310 ± 1310 (h)

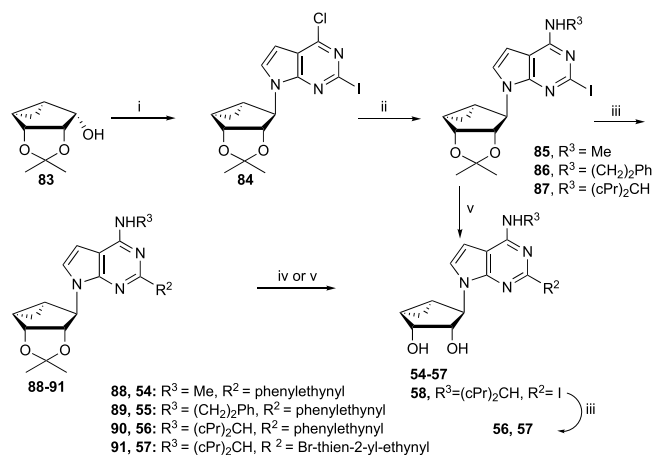
^aDAT and NET binding inhibition is <50% at 10 μM, unless noted. 54: DAT, -58%; 55: NET, K_i = 5.56 μM. ^bBinding assays performed as specified in Table 1, unless noted. Values are expressed as the mean ± SEM (n = 2–4). Values are expressed as the mean ± SEM of N = 2–4 assays performed in duplicate. ^cA₃AR binding data from Tosh et al.^{2,3,6,34,35,37} Representative binding K_i values at hA₁AR (nM): 55, 1300 ± 290; 56, 650 ± 71; determined as reported.³⁷ Values are expressed as the mean ± SEM of N = 3 assays performed in duplicate. ^d30–50% inhibition of radioligand binding at 10 μM. ^e<30% inhibition of radioligand binding at 10 μM.

Scheme 1. Synthesis of 7-Deaza (N)-Methanocarpa 5'-Esters^a



^aReagents and conditions: (i) TIPS, NaH, THF, 0 °C; (ii) 2,2,6,6-tetramethylpiperidine, *n*-BuLi, Bu₃SnCl, THF, -78 °C; (iii) I₂, THF, rt; (iv) TBAF, THF, 0 °C to rt; (v) 7-deaza-2-iodo-6-chloro-purine, Ph₃P, DIAD, THF, rt; (vi) MeNH₂·HCl, Et₃N, MeOH, rt; (vii) 2-chloro or 2-bromo-5-ethynylthiophene, Pd(Ph₃P)₂Cl₂, CuI, Et₃N, DMF, rt; and (viii) 10% TFA, MeOH, 70 °C.

Scheme 2. Synthesis of 4'-Truncated 7-Deaza (N)-Methanocarpa Nucleosides^a



^aReagents and Conditions: (i) 7-Deaza-2-iodo-6-chloro-purine, Ph₃P, DIAD, THF, rt; (ii) R³NH₂, Et₃N, MeOH, rt; (iii) alkynes, Pd(Ph₃P)₂Cl₂, CuI, Et₃N, DMF, rt; (iv) 10% TFA, MeOH, 70 °C; and (v) Dowex 50, MeOH–H₂O, 50 °C

58). Starting with the lead of DOR and TSPO binding reported for compound 4, the truncated N⁶-(3-chlorobenzyl) analogues 3 and 47 with extended C2 groups, and compound 48 that had no C2 substitution, were weaker or inactive in OR binding, but 3 and 47 bound weakly to TSPO. Small N⁶-methyl 49 and ethyl 50 groups or an N⁶-2-phenylethyl 51 group did not produce appreciable OR or TSPO binding. C2-modified analogue 52 and N⁶-(2,2-diphenylethyl) derivative 53 bound measurably at TSPO but not ORs.

7-Deaza-modified truncated analogues were compared: the N⁶-methyl 54, N⁶-(2-phenylethyl) 55 and N⁶-(dicyclopropyl-

methyl) 56 analogues (all C2-phenylethynyl) bound to various ORs in the micromolar range, while 5-bromothien-2-yl-ethynyl derivative 57 bound only to KOR. However, lack of an extended C2 substituent in 58 prevented interaction with both KOR and TSPO. Therefore, as in the 5'-amide series, the 4'-truncated (N)-methanocarba nucleosides bound with moderate affinity at ORs.

Binding assays at NOP⁴¹ indicated moderate-to-weak affinity (K_i , μM) for 4 (4.56 ± 0.45), 9 (>10), 24 (>10), 25 (>10), 28 (3.71 ± 0.78), 29 (2.76 ± 0.67), 35 (>10), 40 (>10), 44 (>10), and 47 (>10). Single-point functional assays at the three ORs, using a TANGO assay of β -arrestin mobilization,⁴² demonstrated that 5'-amide and 5'-ester nucleosides 4, 24, 25, 28, 29, 35, and 45 were antagonists at all three ORs, and no agonist effect was observed at 10 μM at DOR or MOR (Table 6). Agonist activity at KOR was not determined in the

Table 6. Functional Activity at 10 μM (Percent Activity in β -Arrestin-Recruitment TANGO Assay^a Compared with Standard Agonist or Antagonist) at Human ORs^a

no.	DOR		KOR	MOR	
	Ag (%)	Antag (%)	Antag (%)	Ag (%)	Antag (%)
4	-10.3	25.3	125	-1.6	18.8
24	0.7	35.3	58.2	0.3	-13.4
25	-1.7	-6.0	88.1	-1.2	22.6
28	-0.6	85.4	99.6	0.4	96.4
29	-1.1	93.2	104.5	1.6	96.9
35	-1.9	14.1	112.9	3.1	82.1
44	6.7	20.3	65.5	6.0	-44.4

^aDetermined by PDSP, using the Tango GPCR assays as described:⁴² the principle of the assay: receptor activation recruits a β -arrestin fusion protein connected to tobacco etch virus (TEV) protease to the activated OR. The cleavage by TEV protease releases the hybrid factor for transcription GAL4-VP16 from its position fused to the OR. The liberation of the transcription factor induces expression of the β -lactamase reporter gene.⁴⁹ KOR agonist activity was not determined. Values are expressed as the mean \pm SEM of one assay performed in duplicate. The following standard DOR, KOR, and MOR ligands were used for comparison: agonists (set as 100% activation at 10 μM) DAMGO 99, salvinorin A 109, and morphine 110, respectively. Reference antagonist used was naloxone 121 (set as 100% inhibition, at 10 μM), of the effects of corresponding agonist (nM): DOR, DALDE 97; KOR, 109 (3); MOR, 99 (300).

TANGO assay. An additional functional output was determined by conducting dose-response curves at KOR using an enzyme complementation assay to measure β -arrestin2 recruitment to the receptor in U2OS cells (Figure 1). Compounds 28, 39, and 40 inhibited the agonist response of 1 μM *N*-methyl-2-phenyl-*N*-[(5*R*,7*S*,8*S*)-7-(pyrrolidin-1-yl)-1-oxaspiro[4.5]dec-8-yl]acetamide (U69593, 98). Compound 28 was the most potent antagonist with an IC_{50} value equal to 794 ± 50 nM (Table 7). Compounds 43 and 54 did not inhibit agonist 98 in the assay. The compounds were also tested as agonists, and only 43 stimulated β -arrestin2 recruitment and only at the highest concentrations ($30 \pm 4.6\%$ relative to full agonist 98). These compounds were further tested as agonists and antagonists in the KOR-induced $G\alpha_i$ -dependent inhibition of forskolin-stimulated cAMP accumulation (Figure 2). Compounds 28, 39, and 40 inhibited the agonist response of 100 nM 98, with compound 28 again being the most potent antagonist ($\text{IC}_{50} = 2220 \pm 830$ nM, Table 7). Compounds 43 and 54 did not inhibit agonist 98 in

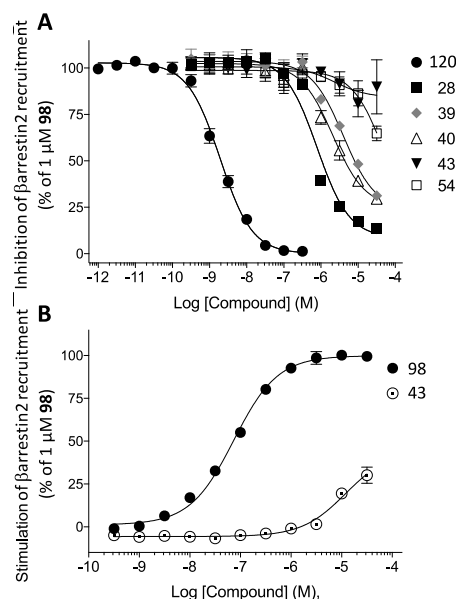


Figure 1. Ligand effects on β -arrestin2 recruitment to hKOR using the DiscoverX PathHunter enzyme fragment complementation assay. (A) Antagonism of stimulated β -arrestin2 recruitment by 1 μM agonist U69593 98. Norbinaltorphimine (NorBNI, 120) is the reference KOR antagonist. (B) Agonist activity; EC_{50} for 98 = 75 ± 9 nM; not derived for 43 due to lack of plateau. $N = 3$ assays performed in duplicate; mean \pm SEM presented.

the assay, and 43 was a weak agonist for KOR-mediated cAMP inhibition ($28 \pm 11\%$ relative to 98).

Activity at the ARs, Transporters, and Other Off-Target Proteins. Some of these nucleoside derivatives, particularly 5'-methylamides, were previously characterized as AR ligands. For example, compound 14 is also a fully efficacious hA₃AR agonist of high affinity ($K_i = 0.70$ nM).² The hA₃AR binding affinities in the series of 5'-esters, such as 23, were consistently in the μM range or weaker, and the affinity at mA₃AR was generally much weaker than at hA₃AR. The hA₁AR and hA_{2A}AR affinities of the nucleosides in this study were generally >10 μM . As reported earlier,⁶ 5'-ester 22 displayed eightfold lower affinity than corresponding 5'-methylamide 14 in hA₃AR binding; thus, the substitution of ester for amide tended to increase both affinity and preference for KOR. The 7-deaza modification of 5'-ethyl ester 28 reduced hA₃AR binding affinity by 31-fold compared with 24, which is greater than the affinity loss in 1-deaza 26 and 3-deaza 27 analogues. Furthermore, 27 and 28 were inactive in mA₃AR binding. 7-Deaza 28 was inactive as an agonist in a functional assay of hA₃AR-mediated inhibition of cAMP formation ($n = 3$),⁴³ with maximal efficacy at 10 μM of $0.59 \pm 6.62\%$, compared with full agonist 5'-*N*-ethyluronamidoadenosine (100%). Thus, the combination of 7-deaza modification with a 5'-small alkyl ester in place of the 5'-amide appears to turn A₃AR agonists into weakly binding A₃AR antagonists or non-A₃AR binding compounds. The functional activity of 5'-esters 22 and 27 as hA₃AR partial agonists was reported.⁶ Therefore, the 5'-ester modification alone reduces A₃AR efficacy, while increasing OR antagonist affinity. A 5'-*n*-propyl ester 30 had higher affinity at both mouse (m) and hA₃ARs than the corresponding 5'-ethyl ester 24, and among the extended esters, 5'-benzyl ester 35 displayed the highest affinity at hA₃AR (K_i 7.81 nM) and at mA₃AR (K_i 891 nM). 4'-Truncated (N)-methanocarba-

Table 7. Antagonism of KOR in the β arrestin2-KOR Enzyme Fragment Complementation Assay (DiscoverX) and cAMP Cisbio Assay^{a,b}

compound	β arrestin2 recruitment		inhibition of cAMP accumulation	
	IC ₅₀ (nM)	Imax (% 120)	IC ₅₀ (nM)	Imax (% 120)
120	2.0 ± 0.3	100	4.0 ± 0.8	100
28	794 ± 50	92 ± 1	2220 ± 830	122 ± 13
39	4200 ± 940	77 ± 3	13100 ± 6000	105 ± 3
40	2220 ± 540	76 ± 2	12100 ± 4400	100 ± 1
43	NC	(10* ± 15)	NC	(23 ± 5)
54	NC	(35* ± 4)	NC	(16 ± 6)

^aData are the mean ± SEM of *N* = 3 Assays Performed in Duplicate (Figures 1 and 2). ^bNC: not converged; (% inhibition at 30 μM). 120 (norbinaltorphimine, nor-BNI) is the reference KOR antagonist.

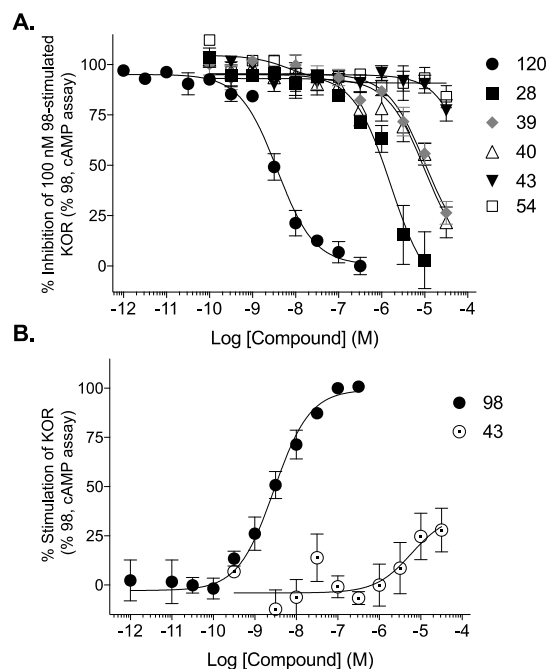


Figure 2. Ligand effects on hKOR-induced inhibition of forskolin-stimulated cAMP accumulation using the Cisbio cAMP Dynamic 2 assay. (A) Antagonism of 100 nM agonist U69593 98-stimulated KOR. NorBNI (120) is the reference KOR antagonist. (B) Agonist activity; EC₅₀ for 98 = 3.3 ± 1.8 nM. Not derived for 43 due to lack of plateau. *N* = 3, performed in duplicate; mean ± SEM presented.

adenosine derivatives displayed varied affinities at hA₃AR, as we previously reported.³⁵ The 7-deaza modification reduced hA₃AR affinity by 16-fold (in a comparison of 54 and 49) or 11-fold (in a comparison of 55 and 51), and the 7-deaza analogues were inactive at the mA₃AR.

Another recently discovered target of certain C2-extended (N)-methanocarba-adenosine derivatives was DAT, as 5'-methyl and ethyl esters in this series were potent allosteric binding enhancers of tropane radioligand affinity (resulting in enhanced level of binding in the primary screen) and inhibitors of dopamine uptake (Figure 3).⁶ Enhancement of radioligand binding at NET was also observed in this chemical series but less potently than at DAT. Thus, it was important to establish effects of the 7-deaza and other modifications on transporters, such as radioligand binding enhancement in the DAT primary screen (Tables 1–3, shown as a negative percent inhibition at 10 μM) and inhibition at NET (Tables 4 and 5). Various 1-, 3- or 7-deaza derivatives (26–29) were compared to probe the participation of these H-bond acceptor nitrogens of adenine

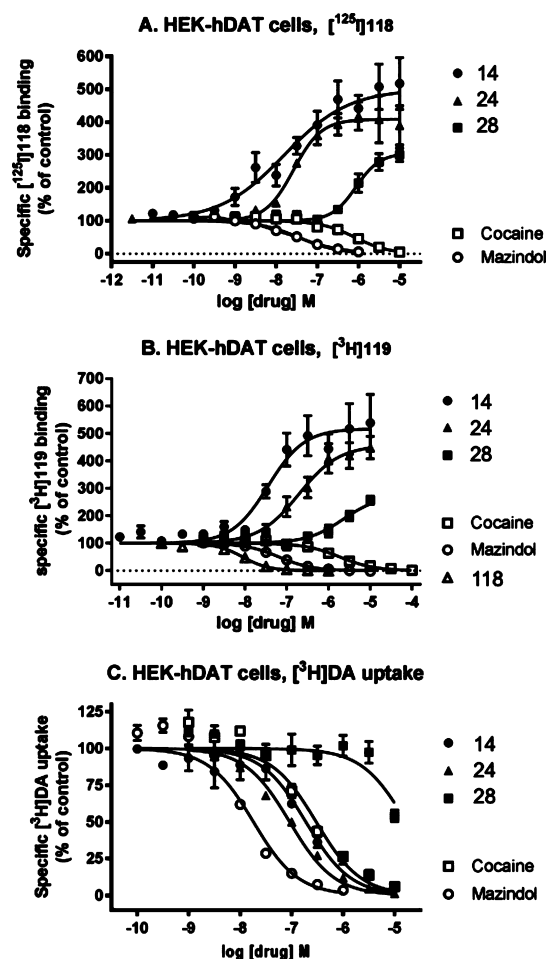


Figure 3. Interaction of selected nucleosides 5'-methylamide 14, 5'-ethyl ester 24, and 7-deaza 5'-ethyl ester 28 as allosteric modulators of hDAT expressed in HEK cells, as characterized using a tropane, methyl (1*R*,2*S*,3*S*)-3-(4-iodophenyl)-8-methyl-8-azabicyclo[3.2.1]octane-2-carboxylate (RTI-55, 118) (A), and a nontropane, (±)-5-(4-chlorophenyl)-3,5-dihydro-2*H*-imidazo[2,1-*a*]isoindol-5-ol (mazindol, 119). (B) Radioligand binding and inhibition of [³H]-dopamine ([³H]DA) uptake (C). Comparison with known binding and uptake inhibitors, cocaine and mazindol, is shown. Methods and data for 14 and 24 were described in Tosh et al.⁶ The 7-deaza modification in 28 greatly reduces the binding enhancement and inhibition of dopamine uptake compared to 24. Compound 30 enhanced DAT binding with an EC₅₀ value of 294 ± 82 nM (not shown). EC₅₀ and IC₅₀ values for the curves shown and archival compounds for comparison are provided in Supporting Information.

for DAT recognition. The 1-deaza modification in the 5'-methylamide series prevented enhancement of tropane radioligand binding at DAT, but not A₃AR binding.^{5,37} Similarly, the conversion of an N⁶-methyl to N⁶-propyl group in **18** greatly reduced DAT interaction, and its 3,3,3-trifluoropropyl equivalent in **19** eliminated it. The corresponding 3-deaza 5'-ethyl ester **27** was nearly as efficacious as **24** in enhancing binding at DAT, whereas the 7-deaza 5'-ester **28** was much less efficacious in enhancing DAT binding. EC₅₀ values for binding enhancement at hDAT determined by the PDSP for **28** and **29** were >10⁻⁶ M. Using an alternate tropane radioligand [¹²⁵I]methyl (1*R*,2*S*,3*S*)-3-(4-iodophenyl)-8-methyl-8-azabicyclo[3.2.1]octane-2-carboxylate (RTI-55, **118**) as described,⁶ **28** enhanced hDAT binding by 320 ± 23% at 10 μM with an EC₅₀ value of 1410 ± 340 nM (Figure 3, Table S1, Supporting Information). Using a nontropane radioligand [³H](±)-5-(4-chlorophenyl)-3,5-dihydro-2*H*-imidazo[2,1-*a*]-isindol-5-ol (mazindol, **119**) as described,⁸ **28** enhanced hDAT binding by a maximal 267 ± 17% with an EC₅₀ value of 2160 ± 550 nM. The IC₅₀ for inhibition of dopamine uptake by **28** was >9800 nM. The potencies in enhancement of binding at hNET and hSERT and in inhibition of uptake were >10 μM. Thus, in the 5'-ester series, the N1 nitrogen atom, but not N3, was essential for interaction with neurotransmitter symporters, and the 7-deaza modification greatly reduced these interactions. Byproducts of the synthesis in the 7-deaza series were inactive at DAT, that is, C2-truncated 5'-methylamide **17** and 5'-butylketone **44**. In the 4'-truncated series, two compounds with C2-phenylethynyl and small N⁶ groups, **49** and **50**, displayed weak-to-moderate DAT interaction, but this binding enhancement disappeared with extension of the N⁶ group in **51**.

The nucleoside derivatives were screened at other off-target interactions by the PDSP (Supporting Information, all values K_i, μM). In addition to those off-target interactions already reported for the archival compounds,^{5,4,6,37} affinity at SHT_{2A} (**27**, 1.30 ± 0.29; **57**, 4.34 ± 1.74), SHT_{2B} (**6**, 2.96 ± 0.60; **27**, 1.78 ± 0.28; **77**, 4.18; **55**, 3.06 ± 0.17; **58**, 1.33), and SHT_{2C} (**21**, 0.51; **23**, 2.33 ± 0.40; **27**, 0.40; **31**, 0.43; **46**, 3.24 ± 1.05; **77**, 0.016) serotonin receptors was detected. Thus, compound **27** bound to all three SHT₂Rs. Curiously, 2',3'-isopropylidene protected compound **77** displayed a high affinity and selectivity (260-fold compared with SHT_{2BR}) at SHT_{2CR}. Compounds **6** and **43** bound to the human α_{2C} adrenergic (6.3 and 0.51, respectively) and compound **6** to the β₃ adrenergic (2.6) receptor. Compound **10** bound to the human SHT_{1A} serotonin (6.3) and β₃ (2.5) receptors. Weak affinity was noted at the muscarinic M₁ (**55**, 6.97) and M₅ (**27**, 3.85) receptors. Compounds **35** and **73** bound to the human SERT (5.56 and 6.58, respectively). Intermediate affinity was found in inhibition of NET binding (**6**, 3.16; **10**, 2.31; **43**, 2.82; **51**, 2.80; **53**, 5.78; **55**, 5.65). Compound **57** bound to the rat brain benzodiazepine receptor with a K_i of 118 nM. Widespread affinity at the rat σ₂ receptor was detected: **6**, 1.54; **10**, 2.51; **26**, 1.76; **36**, 5.87; **42**, 1.11; **47**, 2.73; **51**, 1.48; **52**, 1.82; **56**, 0.67; **57**, 6.92. There were fewer and weaker interactions at the σ₁ receptor: **9**, 7.55; **12**, 7.11; **22**, 8.73; **27**, 1.04; **47**, 7.66.

Molecular Modeling at KOR. Docking and molecular dynamics (MD) were exploited to rationalize the observed experimental data by applying the knowledge gained from the analysis of X-ray structures of KOR, MOR, and DOR with bound antagonists.^{43–45} Although a TSPO X-ray structure was recently reported,⁵² we did not propose a binding mode at this

protein and therefore focused our attention on the molecular signatures determining OR affinity and selectivity. In particular, we generated an initial hypothesis for the KOR binding mode of the 7-deaza 5'-ethyl ester derivative **28** (K_i = 42 nM) and used it to rationalize the SAR of a subset of structurally related analogues (**22**, **24**, **30–37**). Compound **28** was initially docked by Induced Fit Docking (IFD) at a hKOR homology model built upon an available X-ray structure with a bound 4-phenylpiperidine antagonist⁴³ (PDB ID: 4DJH, see Supporting Information). In the resulting docking pose (Figure 4), the

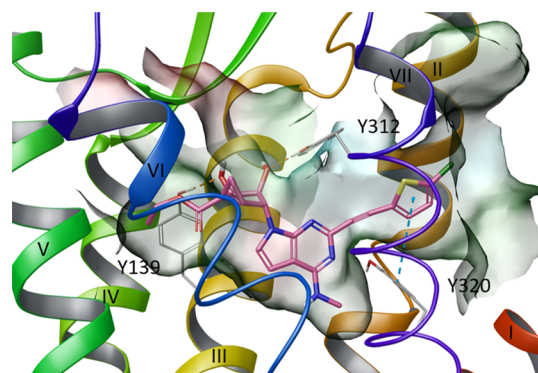


Figure 4. Binding mode predicted by IFD N⁶-methyl 5'-ethylester 7-deaza (N)-methanocarpa derivative **28** (pink carbon atoms, sticks representation) at hKOR. Side chains of residues important for ligand recognition (gray carbon atoms) are reported as sticks. Residues in close contact with the ligand are depicted as transparent surfaces color-coded according to the residue type (red: negatively charged; blue: positively charged; cyan: polar, green: hydrophobic). H-bonds and π–π stacking interactions are pictured as dashed orange and cyan lines, respectively. Nonpolar hydrogen atoms are omitted. The PDB ID of the X-ray structure used as starting points for molecular modeling was 4DJH.

ligand resided in the upper portion of the TM (transmembrane) bundle with the (N)-methanocarpa ring pointing toward the EC side and the N⁶-methyl group buried in the binding cleft. The C2 extension was directed toward a Tyr-rich region at the interface of TM2, TM1, and TM7. The ligand established interactions with residues located mainly in TM3, TM6, and TM7, consisting of two H-bond interactions of the C3' and the C2' hydroxyl groups with the side chains of Tyr312 (7.35) and Tyr139 (3.33), respectively, and π–π stacking interaction between the 5-chlorothiophenyl moiety and the side chain of Tyr320 (7.43). Surprisingly, the ligand did not form a H-bond with the conserved Asp138 (3.32) residue.

We subjected the initial docking pose of **28** to 30 ns of membrane MD simulation (run in triplicate). Replicas were run by using different initial randomly assigned atom velocities, and ligand–receptor interactions were analyzed qualitatively (ligand and protein root-mean-square deviation (RMSD) values in Table S2). We considered a key His residue surrounding the binding site, that is, His291 (6.52), in two possible alternative protonation states and compared the two result sets (Video S1). A preliminary analysis of the His(6.52) environment in the available antagonist-bound KOR,⁴³ MOR (PDB ID: 4DKL),⁴⁴ and DOR (PDB ID: 4N6H)⁴⁵ X-ray structures unequivocally determined it as protonated on the N^ε atom (hereby denoted as HSE), as the residue established a H-bond with the aromatic hydroxyl moiety of the co-crystallized antagonists mediated by two highly conserved water molecules. As we did not retain those water molecules during the IFD and

the binding mode of **28** (Figure 4) did not predict the presence of a H-bond donor moiety in proximity to His291 (6.52), we also considered the alternative protonation state featuring a hydrogen atom on the N^δ (hereby denoted as HSD).

Notably, in all the simulations run with both HSE and HSD models, the ligand moved deeper in the binding site with respect to the initial docking pose to establish a persistent H-bond between the 3'-OH group and the conserved Asp138 (3.32) side chain. However, as reported in Table S2 and visualized in Video S1 (right panel), in the HSD model, the ligand was characterized by a higher average RMSD value and was less stable. By superimposing the lowest interaction energy (IE) complexes extracted for each replica of the two models (Figure 5A,B), it was evident that TM1, which was

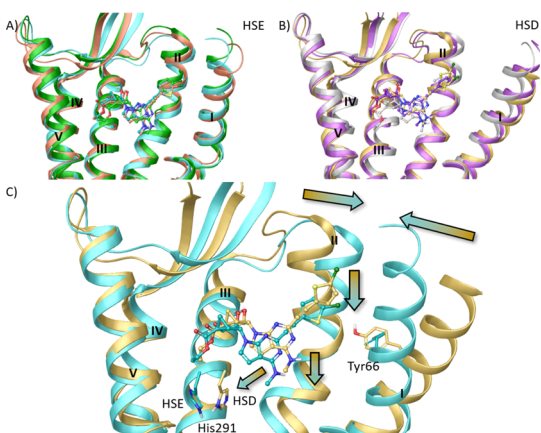


Figure 5. Superimposition of ligand–protein complexes characterized by lowest IE values during the MD simulation (replicas represented with different colors) of (A) HSE and (B) HSD hKOR models in complex with N^δ-methyl 5'-ethylester 7-deaza (N)-methanocarpa derivative **28** (ball and sticks representation). (C) Superimposition of ligand–protein complexes characterized by lowest IE values among three replicas (see Table S2) for the HSE (cyan ribbon, and ligand in cyan ball and sticks) and the HSD (yellow ribbons, ligand in yellow ball and sticks) hKOR models in complex with N^δ-methyl 5'-ethylester 7-deaza (N)-methanocarpa derivative **28**. Side chains of residues undergoing considerable conformational changes during the MD simulation are highlighted (sticks representation with carbon atoms matching the color of the model). Arrows indicate the shift of ligand position and TMs between the two models. TM6, EL3, and TM7 were omitted to aid visualization. The PDB coordinates of both complexes are available as separate Supporting Information files. The PDB ID of the X-ray structure used as starting points for molecular modeling was 4DJH.

considerably displaced with respect to the TM bundle in the initial X-ray structure,⁴³ maintained its displaced position in the HSD model and approached the TM bundle in the HSE model. To investigate the reason for the different placement of TM1 in the two models, we analyzed in more detail a selected trajectory for each model (Table S6 and Video S1) and focused our attention on the ligand–protein complexes characterized by the lowest IE value extracted from each trajectory. As depicted in Figure 5C, in the HSD model, His291 (6.52) rotated and pointed toward TM3. This rotation was accompanied by the diffusion of water molecules into the binding cavity that connected His291 (6.52) to the conserved Asp138 (3.32) (Video S1, right panel). The presence of this network of water molecules pushed the ligand slightly higher in

the binding site. In the HSE model, His291 (6.52) maintained its initial conformation facing TMS, thus allowing the ligand to be accommodated deeper in the binding site (Video S1, left panel). Concerning the placement of TM1 with respect to the TM bundle, in the HSE model, the movement of TM1 occurred early during the equilibration phase (data not shown) and was triggered by favorable hydrophobic interactions established by 5-chlorothieryl moiety of the ligand with residues at the interface between TM1 (Ile62) and TM2 (Tyr119), which persisted during the production phase (Video S1, left panel).

Considering both higher ligand stability in the MD simulations and the analysis of the X-ray structures,^{43–45} we considered the HSE model more reliable and inspected the ligand environment in the selected trajectory more carefully. In the ligand–protein complex characterized by the lowest IE values (Figure 6), the ligand was almost completely buried and

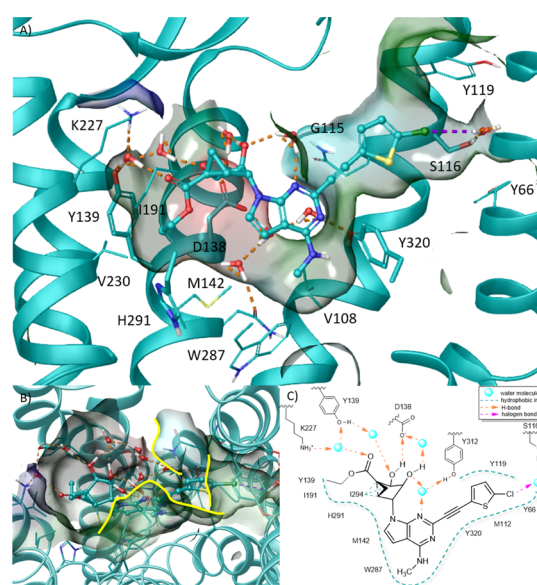


Figure 6. (A) Side view, (B) top view, and (C) schematic representation of the hypothetical binding mode of N^δ-methyl 5'-ethylester 7-deaza (N)-methanocarpa derivative **28** (cyan carbon atoms, ball and sticks representation) at hKOR as predicted by MD simulation. Side chains of residues important for ligand recognition (cyan carbon atoms) and water molecules are represented as sticks. Residues in close contact with the ligand are depicted as transparent surfaces color-coded according to the residue type (red: negatively charged; blue: positively charged; cyan: polar, green: hydrophobic) with boundaries to solvent exposure highlighted with yellow solid lines. H-bonds and halogen bonds are pictured as dashed orange and purple lines, respectively. Nonpolar hydrogen atoms are omitted. TM6, EL3, and TM7 were omitted to aid visualization. The PDB ID of the X-ray structure used as starting points for molecular modeling was 4DJH.

shielded from the aqueous environment, except for the 2',3'-OH groups and the 5'-carbonyl group (Figure 6B). Consequently, the interactions involving those groups were mainly direct and water-mediated H-bonds established with polar residues (Figure 6A,C). The C3' group established an H-bond with the conserved Asp138 (3.32) and a water-mediated H-bond with Tyr139 (3.33). The C2' hydroxyl was H-bonded to the conserved Asp138 (3.32) through the interplay of another water molecule. Additional water molecules connected the N3 nitrogen to the C2' hydroxyl group and the side chain

of Tyr312 (7.37) and the 5'-carbonyl group to the side chains of Tyr139 (3.33) and Lys227 (5.39). The 5'-ethyl ester moiety was accommodated in a small hydrophobic pocket delimited by Met142 (3.36), Tyr139 (3.33), and Val230 (5.42). The N⁶-methyl group was hosted in a hydrophobic pocket delimited by the conserved Trp187 (6.48), and the fused cyclopropyl ring of the (N)-methanocarpa system established hydrophobic contacts with Ile194 (6.55). The 5-chlorothienyl moiety lay in a hydrophobic pocket delimited by Tyr312 (7.35), Tyr119 (2.64), Tyr66 (1.39), Met112 (2.57), and Tyr320 (7.43) with a water-mediated halogen bond interaction connecting the chlorine atom to the side chain of Ser116 (2.61).

We finally tested the ability of the binding hypothesis suggested by MD simulation (Figure 6) in rationalizing the SAR at KOR of a subset of structurally related ligands, namely, 7-aza **22**, **24**, and **30**–**37**. In the corresponding docking poses (Figure 7), all ligands maintained the above described pattern

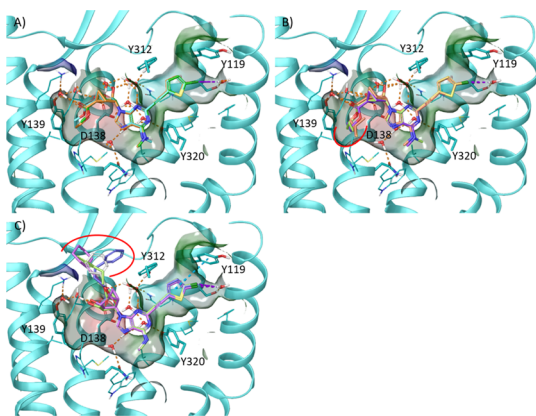


Figure 7. Docking poses of 7-aza 5'-ester (N)-methanocarpa derivatives at the hKOR. (A) Predicted docking poses of **22** (green carbon atoms), **24** (cyan carbon atoms), and **30** (orange carbon atoms). (B) Predicted docking poses of **30** (purple carbon atoms), **31** (green carbon atoms), **32** (yellow carbon atoms), and **33** (orange carbon atoms). (C) Predicted docking poses of **34** (magenta carbon atoms), **35** (gray carbon atoms), **36** (green carbon atoms), and **37** (blue carbon atoms). Side chains of residues important for ligand recognition (cyan carbon atoms) and water molecules are represented as sticks. Residues in close contact with the ligand are depicted as transparent surfaces color-coded according to the residue type (red: negatively charged; blue: positively charged; cyan: polar, green: hydrophobic). H-bonds, π - π stacking interactions and halogen bonds are pictured as dashed orange, cyan, and purple lines, respectively. Nonpolar hydrogen atoms are omitted. Red solid lines highlight the changes with respect to the binding mode predicted for the 7-deaza derivative **28** (Figure 3). TM6, EL3, and TM7 were omitted to aid visualization. The PDB ID of the X-ray structure used as starting points for molecular modeling was 4DJH.

of H-bond interactions while differing in the 5'-ester group placement. The docking analysis suggested that the hKOR affinity modulation arises from the ability of this group to fit the narrow hydrophobic pocket delimited by Met142 (3.36), Val230 (5.42), and Tyr139 (3.33). In particular, the hydrophobic contact of the ester with Tyr139 (3.33) seems to favorably modulate the KOR binding affinity, as the 7-aza methyl-ester derivative **22** ($K_i = 3130$ nM) binds in a pose that superimposes well with the one predicted for **28** ($K_i = 42$ nM) and **24** ($K_i = 396$ nM) but lacks this interaction (Figure 7A). Slight elongation of the alkyl ester chain is moderately tolerated, whereas further alkyl elongation/branching or the

introduction of aliphatic/aromatic cycles requires the position of the bulkier groups to be either outside the above-mentioned hydrophobic pocket (Figure 7B) or completely solvent exposed (Figure 7C), respectively.

Concerning the hKOR affinity increase and the display of MOR and DOR affinity in 7-deaza derivatives, we speculate that the presence of a 7-nitrogen atom would trap unstable water molecules in the small pocket delimited by the conserved Trp287 (6.48), thus disrupting the hydrophobic contacts with the N⁶-methyl and the C7 atom. Although we were not able to confirm this hypothesis, the MD simulation of the HSD model clearly suggested the presence of ligand-destabilizing water molecules in this binding cavity region. Moreover, the superimposition between the proposed hKOR binding mode and the WaterMap computed by Goldfeld et al. on the KOR X-ray structure⁹ (Figure S7) highlighted that the hydrophobic moieties of **28**, such as the 5'-ethyl ester, the 7-deaza position, the N⁶-methyl group and the C2-(5-chlorothien-2-yl-ethynyl) moiety, overlapped well with regions predicted to be occupied by "unhappy" water molecules. On the other hand, the N1 and N3 adenine nitrogen atoms, the 5'-carbonyl group, and the C2' and C3' hydroxyl groups lie close to a region rich in "happy" water molecules.

Finally, our modeling analysis also suggested that the moderate hKOR preference might arise from a water-mediated H-bond between the N3 nitrogen and the non-conserved Tyr312 (7.35). Binding data suggested that a 3-deaza modification might be incompatible with the ORs as it clearly caused a loss of hKOR affinity (e.g., **24** vs its 3-deaza analogue **27**, $K_i = 396$ nM and % of control at 10 μ M < 10%, respectively). However, further derivatives need to be synthesized and tested to fully support this speculation.

ADME-Tox Testing. The in vivo pharmacokinetics of **28** was studied in the Sprague-Dawley rat (Figure 8 and Table S3), and in vitro preclinical testing was performed using described methods (Supporting Information).⁵ Upon oral administration of 1, 5, and 10 mg/kg doses, the bioavailability was determined to be 58, 92, and 60 % F, respectively. Furthermore, in vitro

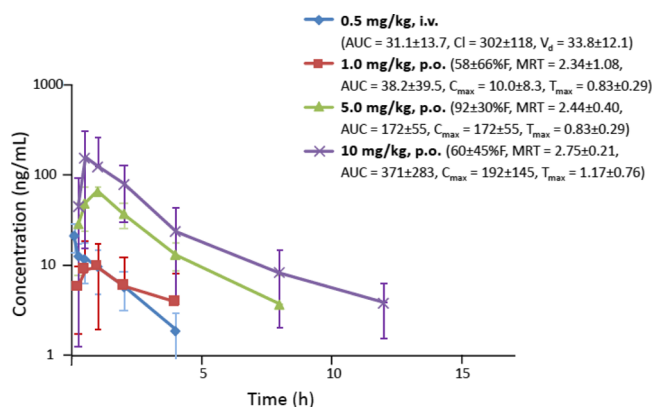


Figure 8. Pharmacokinetics of **28** in male SD rats. Rats were fasted overnight for three oral doses, but fed for the i.v. dose. The in vivo half-life ($t_{1/2}$, h, p.o.) of **28** was 1 mg/kg, 2.16 ± 0.45; 3 mg/kg, 1.55 ± 0.42; 10 mg/kg, 1.91 ± 0.28. The $t_{1/2}$ for the i.v. dose was 1.31 ± 0.06 h. Oral bioavailability (% F) and other pharmacokinetic parameters (units) are indicated: MRT (mean residence time, h); AUC (area under the curve, time 0 to ∞ , ng·h/mL); CI (clearance, mL/min/kg); V_d (volume of distribution, L/kg); $C_{max} = 10.0 \pm 8.3$ (max. concentration, ng/mL); T_{max} (time at max. concentration, h).

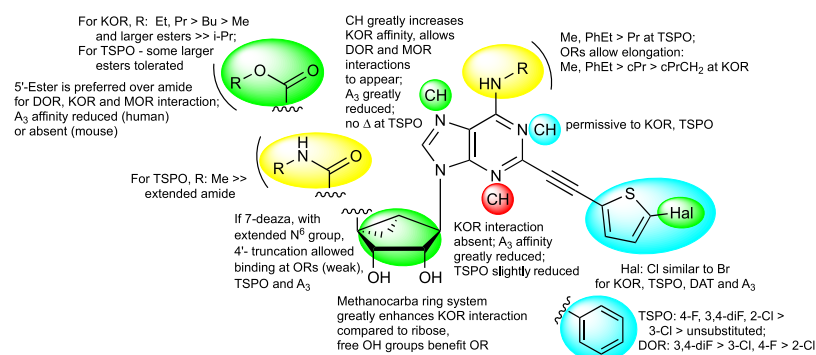


Figure 9. SAR summary at ORs, TSPO, and A₃AR of rigid (N)-methanocarba nucleosides from binding data.

preclinical testing (Tables S4–S7, Figures 8 and 9) demonstrated that **28** was not an inhibitor of hERG ($IC_{50} > 30 \mu\text{M}$, using a fluorescence polarization assay) or CYP450 enzymes ($IC_{50} \geq 10 \mu\text{M}$ at 1A2, 2C9, 2C19, 2D6 and 3A4 isoforms) or cytotoxic to Hep-G2 cells ($CC_{50} > 30 \mu\text{M}$). It was stable in human plasma (98% remaining after 2 h) and in simulated gastric and intestinal fluids (100% remaining after 240 min). The CACO-2 cell permeability (P_{app} , apical to basal) was 1.42×10^{-6} cm/s, with efflux indicated (ratio 15.6).

DISCUSSION

The affinities of the present nucleoside derivatives are not comparable to the most potent indolyl or tetrahydroquinolyl antagonists of KOR⁴³ or sub nM antagonists of MOR or to known ligands of TSPO,^{25,28,29} but nucleosides represent a novel scaffold for the ORs and possibly TSPO. However, to effectively repurpose this versatile scaffold, it was desired to reduce the A₃AR affinity, and in some cases A₃AR agonist efficacy was also reduced, while enhancing KOR affinity. Furthermore, activity at other sites, such as inhibition of binding at NET or enhancement of binding at DAT was observed in some derivatives. Thus, a major challenge in this study was to identify principles of preference for KOR, which was largely accomplished in the 7-deaza 5'-ethyl ester series.

In general, affinity at both KOR and TSPO was evident in this series with extended C2 substituents, with weaker activity at DOR and MOR (Figure 9). Nevertheless, an affinity correlation plot (Figure S6) showed no direct correlation between KOR and TSPO, and we have no reason to expect a binding site structural similarity. One of the most potent ligands in KOR binding **28** (ligand efficiency = 0.25) was consistently the most potent KOR antagonist tested in two functional assays, that is, to block the activity of a reference agonist (**98**, U69593, nor-BNI) in β arrestin2-dependent and Gi-protein-dependent signaling. Among 5'-methylamides, the TSPO ligands with highest binding affinity (K_i 200–300 nM) were the 3,4-diF-Ph **4**, 4-F-Ph **7**, and 2-Cl-Ph **8** analogues,⁷ but not 3-chloro **9**. However, we also functionalized the molecules in a manner to distinguish between the two receptor classes. Compound **14** bound with moderate affinity at TSPO and was inactive at ORs. Among the more potent KOR antagonists, 7-deaza compounds **28** and **29** bound to both ORs and TSPO, but ester group extension greatly reduced the TSPO affinity. Also, compounds **39** and **40** with a modified C2 substitution and the unusual 2',3'-isopropylidene intermediate **82** bound with a preference for KOR compared with TSPO. Binding at the ORs was sensitive to the terminal ring of the C2 substituent. The C2-phenylethynyl group provided a slightly

greater preference than C2-5-chlorothienylethynyl for KOR with respect to TSPO.

Ribose analogues **45** and **46** were inactive at ORs and TSPO, although they corresponded to (N)-methanocarba analogues that bound to TSPO (**14**) or KOR (**22**). The equivalent 9-unsubstituted adenine nucleobase moiety of **3** and **4** did not bind appreciably to TSPO or ORs ($K_i > 10 \mu\text{M}$).⁶ Thus, the pseudoribose moiety is needed for interaction at these sites. The rigid (N)-methanocarba ring promoted interaction with these receptors, possibly by maintaining a specific receptor-preferred conformation of this pseudoribose moiety.

There is an overlap in the nucleoside structures that act allosterically at DAT (e.g., **14** and **24**) and those that inhibit KOR binding. As for the KOR binders, a 5'-ester group favored DAT interaction. However, changing the size of the 5'-ester group was a means of separating those activities. While both 5'-methyl and ethyl esters acted at DAT, the 5'-methyl ester was inactive at KOR. The larger (5'-propyl and beyond) esters were less potent and efficacious than smaller esters in enhancing tropane radioligand binding at DAT but retained some KOR affinity. The 5'-propyl ester **30** enhanced human DAT binding with an EC_{50} value of 294 ± 82 nM, which is less potent than the 5'-ethyl ester **24** (EC_{50} 34 ± 13 nM).³³ Thus, even in the 7-aza series, we have partially separated the activity at KOR from interactions with other receptors and transporters.

We have shown that a 3-deaza modification removed OR affinity, but TSPO interaction is still present. Compound **28** had an 11-fold preference for binding at KOR versus TSPO. The 1-deaza (**26**) and to some extent the 7-deaza (**28** and **29**) modifications are a means of eliminating DAT interaction in this series. The most effective means of separating OR binding affinity relative to other sites of action, that is, DAT and ARs, is the 7-deaza modification. However, many 7-deaza nucleosides here also bound to TSPO. A 5-bromothien-2-yl-ethynyl group prevented TSPO binding in the 5'-amide but not 5'-ester or 4'-truncated series. Curiously, various nucleosides with large N⁶ substituents (e.g., N⁶-2-phenylethyl in **43**, **51**, and **55**) weakly inhibited NET binding, rather than enhancing it as seen in radioligand assays with reference compounds **14** and **24**.

Truncation of the 5'-amide or ester group was compatible with moderate binding at TSPO and weaker binding at ORs. The most potent truncated ligands (K_i , nM) at TSPO were **52** (877) and **57** (353). The most potent truncated ligands (K_i , nM) were **54** (1120) and **55** (1130) at KOR and **56** (1440) at MOR (all C2-phenylethynyl 7-deaza analogues). We expect the 4'-truncated analogues to bind to ORs in a similar

orientation as the full nucleosides, but without the 5'-group (fitting a narrow hydrophobic pocket) the ligands are likely not well anchored in the binding site.

There is a possibility that a compound acting centrally as both KOR antagonist and dopamine uptake inhibitor could have a beneficial, synergistic antidepressant effect based on these two mechanisms. KOR activation reduces the availability of dopamine in the brain, and KOR agonists induce depression.^{16,46} However, we have not evaluated the benefit of additivity of activities of these nucleosides at receptors, channels, and transporters.

We have demonstrated oral bioavailability of the KOR antagonist **28**. The presence of an ester group that is conducive to high OR affinity in the present chemical series might be predictive of a short in vivo half-life. However, the half-life (1.6–2.2 h) or mean residence time (2.3–2.8 h) of **28** (p.o.) in rats did not indicate rapid hydrolysis.¹⁷ A similar result was obtained with a different series of (N)-methanocarba nucleosides containing 5'-esters and 5'-amides;²⁵ thus, the ester functionality in this (N)-methanocarba nucleoside series appears to be sterically protected from hydrolysis by the adjacent bicyclic ring system.

Furthermore, we have not evaluated the ability of these relatively complex nucleosides to cross the blood–brain barrier. However, except for carrier-mediated transport of simple adenosine derivatives by the equilibrative nucleoside transporter1, nucleoside derivatives that are derivatized at the N⁶ and C2 positions for potent interaction with GPCRs tend not to readily cross the blood–brain barrier, as indicated by a study of A₁AR agonists.⁴⁷ The potential use of OR antagonists acting peripherally for cancer treatment has been proposed, based on experiments in MOR-knockout mice and an unplanned post hoc analysis of patients receiving MOR antagonist methylnaltrexone parenterally for OIC.⁴⁸ Thus, there are applications for selective OR antagonists in the periphery. Further study of these OR antagonists is needed to determine if their action is predominantly in the periphery when administered orally or i.p.

CONCLUSIONS

In conclusion, as with our previous reports on repurposing the (N)-methanocarba scaffold from ARs to 5HT_{2B} and 5HT_{2C} receptors and the DAT,^{6,7} we now show that moderate affinity at KOR within the same chemical series is achievable. The current findings expand our hypothesis that these rigid nucleosides are indeed privileged structures.⁴ The highest affinity as KOR antagonist achieved was ~40 nM for 7-deaza ethyl esters **28** and **29**, which displayed at least an order of magnitude preference at KOR, including in comparison to the A₃AR and TSPO. Moreover, leads for ligands that bind at DOR, MOR, and even NOP have been identified, and the KOR affinity and selectivity of this repurposed scaffold could potentially be enhanced in future studies. Unlike many of the known OR antagonists, these conformationally locked nucleosides interact potently with KOR in the absence of a free basic amino group, which is present in the native ligands. The rigidity of this chemical series was exploited in the molecular modeling of the KOR interaction of **28** using MD simulations. Thus, we have repurposed a ligand class designed originally for one GPCR to a different class of GPCRs and analyzed its KOR interactions structurally in a coherent manner.

EXPERIMENTAL PROCEDURES

Chemical Synthesis. Materials and Instrumentation. Similar syntheses of (N)-methanocarba nucleosides have been reported.^{2,3,5,6,33,35,38} Sigma-Aldrich (St. Louis, MO) was the source for most of the reagents and solvents. Other reagents were purchased from Small Molecules, Inc. (Hoboken, NJ), Anichem (North Brunswick, NJ), PharmaBlock, Inc. (Sunnyvale, CA), Frontier Scientific (Logan, UT), and Tractus (Perrineville, NJ). ¹H NMR spectra were measured on a Bruker 400 spectrometer with CDCl₃, CD₃OD, or dimethyl sulfoxide as solvent. Chemical shifts are given as δ values in ppm from the standard tetramethylsilane signal set at 0.00 when CDCl₃ was used as solvent and the water peak at δ 3.30 when CD₃OD was used as a solvent. A Bruker AV spectrometer equipped with a z-gradient [¹H, ¹³C, ¹⁵N]-cryoprobe was used. Analytical thin layer chromatography analysis was performed using silica gel F254 (0.2 mm) coated on glass plates (Sigma-Aldrich, St. Louis, MO). The purity of the terminal nucleoside derivatives was analyzed by high-performance liquid chromatography (HPLC) (1100 series, Agilent Technologies Inc., Palo Alto, CA) using as a column Agilent Zorbax SB, 50 × 4.6 mm, with a mobile phase consisting of a linear gradient (80:20 to 0:100 in 13 min) of 5 mM TBAP (tetrabutylammonium dihydrogenphosphate) to CH₃CN with a 0.5 mL/min flow. UV diode array detection was followed at 230, 254, and 280 nm. The final product nucleosides tested biologically displayed >95% HPLC purity (254 nm). Routine mass spectrometry (MS) was performed using a JEOL SX102 spectrometer with 6 kV Xe atoms following desorption from a glycerol matrix or LC/MS 1100 MSD (Agilent), equipped with an Atlantis C18 column (Waters, Milford, MA). High-resolution MS (HRMS) was performed using a Q-TOF-2 (Micromass-Waters), calibrated (external polyalanine calibration) for proteomics was used. Observed accurate masses (uncorrected for temporal drift) are as expected, consistent with instrumental performance and standard compounds' mass trends maintained over time.

Ethyl(1S,2R,3S,4R,5S)-4-(2-((5-chlorothiophen-2-yl)ethynyl)-4-(methylamino)-7H-pyrrolo[2,3-d]pyrimidin-7-yl)-2,3-dihydroxybicyclo[3.1.0]hexane-1-carboxylate (28). TFA (10%, 3 mL) was added to a solution of compound **77** (74 mg, 0.144 mmol) in MeOH (3 mL) and heated at 70 °C for 3 h. The solvent was evaporated, and the residue was purified on flash silica gel column chromatography (CH₂Cl₂/MeOH = 30:1) to give the compound **28** (60 mg, 89%) as a syrup. ¹H NMR (CD₃OD, 400 MHz): δ 7.30 (d, *J* = 4.4 Hz, 1H), 7.03 (d, *J* = 4.4 Hz, 1H), 7.01 (d, *J* = 4.0 Hz, 1H), 6.61 (d, *J* = 3.6 Hz, 1H), 5.12 (d, *J* = 6.4 Hz, 1H), 5.04 (s, 1H), 4.29–4.21 (m, 2H), 3.92 (d, *J* = 6.4 Hz, 1H), 3.09 (s, 3H), 2.10–2.07 (m, 1H), 1.96 (t, *J* = 5.2 Hz, 1H), 1.66–1.62 (m, 1H), 1.30 (t, *J* = 7.2 Hz, 3H). HRMS calcd for C₂₂H₂₂N₄O₄SCl (M + H)⁺: 473.1050; found, 473.1043.

Ethyl(1S,2R,3S,4R,5S)-4-(2-((5-bromothiophen-2-yl)ethynyl)-4-(methylamino)-7H-pyrrolo[2,3-d]pyrimidin-7-yl)-2,3-dihydroxybicyclo[3.1.0]hexane-1-carboxylate (29). Compound **29** (85%) was prepared from compound **78** by adapting the method provided for compound **28**. ¹H NMR (CD₃OD, 400 MHz): δ 7.26 (d, *J* = 4.0 Hz, 1H), 7.14 (d, *J* = 4.0 Hz, 1H), 7.03 (d, *J* = 3.6 Hz, 1H), 6.61 (d, *J* = 3.6 Hz, 1H), 5.11 (d, *J* = 5.2 Hz, 1H), 5.02 (s, 1H), 4.29–4.21 (m, 2H), 3.92 (d, *J* = 5.2 Hz, 1H), 3.09 (s, 3H), 2.10–2.07 (m, 1H), 1.96 (t, *J* = 5.2 Hz, 1H), 1.66–1.62 (m, 1H), 1.30 (t, *J* = 7.2 Hz, 3H).

HRMS calcd for $C_{22}H_{22}N_4O_4SBr$ ($M + H$)⁺: 517.0545; found, 517.0548.

Ethyl(1S,2R,3S,4R,5S)-2,3-dihydroxy-4-(2-iodo-4-(methylamino)-7H-pyrrolo[2,3-d]pyrimidin-7-yl)bicyclo[3.1.0]hexane-1-carboxylate (39). Compound **39** (90%) was prepared from compound **73** by adapting the method provided for compound **28**. ¹H NMR (CD₃OD, 400 MHz): δ 6.8 (d, *J* = 3.6 Hz, 1H), 6.52 (br s, 1H), 5.15 (d, *J* = 6.8 Hz, 1H), 4.92 (s, 1H), 4.29–4.21 (m, 2H), 3.92 (d, *J* = 6.8 Hz, 1H), 3.03 (br s, 3H), 2.04–2.01 (m, 1H), 1.89 (t, *J* = 5.2 Hz, 1H), 1.62–1.59 (m, 1H), 1.31 (t, *J* = 7.2 Hz, 3H). HRMS calcd for $C_{16}H_{20}N_4O_4I$ ($M + H$)⁺: 459.0529; found, 459.0521.

Ethyl(1S,2R,3S,4R,5S)-2,3-dihydroxy-4-(4-(methylamino)-2-(phenylethynyl)-7H-pyrrolo[2,3-d]pyrimidin-7-yl)bicyclo[3.1.0]hexane-1-carboxylate (40). Compound **40** (87%) was prepared from compound **79** by adapting the method provided for compound **28**. ¹H NMR (CD₃OD, 400 MHz): δ 7.68–7.66 (m, 2H), 7.45–7.43 (m, 3H), 7.05 (d, *J* = 3.6 Hz, 1H), 6.64 (d, *J* = 3.6 Hz, 1H), 5.13 (d, *J* = 5.6 Hz, 1H), 5.05 (s, 1H), 4.29–4.21 (m, 2H), 3.83 (d, *J* = 5.6 Hz, 1H), 3.12 (s, 3H), 2.11–2.08 (m, 1H), 1.97 (t, *J* = 5.2 Hz, 1H), 1.66–1.63 (m, 1H), 1.30 (t, *J* = 7.2 Hz, 3H). HRMS calcd for $C_{24}H_{23}N_4O_4$ ($M + H$)⁺: 433.1876; found, 433.1879.

Ethyl(1S,2R,3S,4R,5S)-4-(4-(cyclopropylamino)-2-(phenylethynyl)-7H-pyrrolo[2,3-d]pyrimidin-7-yl)-2,3-dihydroxybicyclo[3.1.0]hexane-1-carboxylate (41). Compound **41** (85%) was prepared from compound **80** by adapting the method provided for compound **28**. ¹H NMR (CD₃OD, 400 MHz): δ 7.68–7.66 (m, 2H), 7.45–7.43 (m, 3H), 7.07 (d, *J* = 3.6 Hz, 1H), 6.78 (br s, 1H), 5.14 (d, *J* = 7.2 Hz, 1H), 5.06 (s, 1H), 4.29–4.19 (m, 2H), 3.94 (d, *J* = 6.8 Hz, 1H), 3.02–2.97 (m, 1H), 2.11–2.08 (m, 1H), 1.97 (t, *J* = 5.2 Hz, 1H), 1.67–1.63 (m, 1H), 1.30 (t, *J* = 7.2 Hz, 3H), 0.95–0.90 (m, 2H), 0.71–0.67 (m, 2H). HRMS calcd for $C_{26}H_{27}N_4O_4$ ($M + H$)⁺: 459.2032; found, 459.2027.

Ethyl(1S,2R,3S,4R,5S)-4-(4-((cyclopropylmethyl)amino)-2-(phenylethynyl)-7H-pyrrolo[2,3-d]pyrimidin-7-yl)-2,3-dihydroxybicyclo[3.1.0]hexane-1-carboxylate (42). Compound **42** (84%) was prepared from compound **81** by adapting the method provided for compound **28**. ¹H NMR (CD₃OD, 400 MHz): δ 7.67–7.65 (m, 2H), 7.44–7.43 (m, 3H), 7.04 (d, *J* = 3.6 Hz, 1H), 6.73 (d, *J* = 3.6 Hz, 1H), 5.13 (d, *J* = 6.8 Hz, 1H), 5.05 (s, 1H), 4.29–4.21 (m, 2H), 3.93 (d, *J* = 6.4 Hz, 1H), 3.47 (d, *J* = 6.8 Hz, 2H), 2.12–2.08 (m, 1H), 1.97 (t, *J* = 5.2 Hz, 1H), 1.66–1.62 (m, 1H), 1.30 (t, *J* = 7.2 Hz, 3H), 1.25–1.16 (m, 1H), 0.60–0.55 (m, 2H), 0.36–0.33 (m, 2H). HRMS calcd for $C_{27}H_{29}N_4O_4$ ($M + H$)⁺: 473.2189; found, 473.2189.

Ethyl(1S,2R,3S,4R,5S)-2,3-dihydroxy-4-(4-(phenethylamino)-2-(phenylethynyl)-7H-pyrrolo[2,3-d]pyrimidin-7-yl)bicyclo[3.1.0]hexane-1-carboxylate (43). Compound **43** (87%) was prepared from compound **82** by adapting the method provided for compound **28**. ¹H NMR (CD₃OD, 400 MHz): δ 7.68–7.67 (m, 2H), 7.46–7.44 (m, 3H), 7.30–7.29 (m, 4H), 7.22–7.19 (m, 4H), 7.09 (d, *J* = 3.6 Hz, 1H), 6.69 (d, *J* = 3.6 Hz, 1H), 5.14 (d, *J* = 6.8 Hz, 1H), 5.05 (s, 1H), 4.26–4.21 (m, 2H), 3.96 (d, *J* = 6.8 Hz, 1H), 3.85 (t, *J* = 7.2 Hz, 2H), 3.02 (t, *J* = 7.2 Hz, 2H), 2.12–2.08 (m, 1H), 1.96 (t, *J* = 5.2 Hz, 1H), 1.67–1.63 (m, 1H), 1.29 (t, *J* = 7.2 Hz, 3H). HRMS calcd for $C_{31}H_{31}N_4O_4$ ($M + H$)⁺: 523.2345; found, 523.2348.

(1R,2R,3S,4R,5S)-4-(4-(Methylamino)-2-(phenylethynyl)-7H-pyrrolo[2,3-d]pyrimidin-7-yl)bicyclo[3.1.0]hexane-2,3-

diol (54). TFA (10%, 2 mL) was added to a solution of compound **88** (20 mg, 0.05 mmol) in MeOH (2 mL) and heated at 70 °C for 3 h. The solvent was evaporated, and the residue was purified on flash silica gel column chromatography (ethylacetate/MeOH = 50:1) to give the compound **54** (16 mg, 90%) as a colorless syrup. ¹H NMR (CD₃OD, 400 MHz): δ 7.68–7.66 (m, 2H), 7.47–7.43 (m, 3H), 7.36 (d, *J* = 3.6 Hz, 1H), 6.68 (s, 1H), 5.07 (s, 1H), 4.69 (br s, 1H), 3.77 (d, *J* = 6.4 Hz, 1H), 3.15 (s, 3H), 1.99–1.96 (m, 1H), 1.63–1.59 (m, 1H), 1.38–1.35 (m, 1H), 0.77–0.72 (m, 1H). HRMS calcd for $C_{21}H_{21}N_4O_2$ ($M + H$)⁺: 361.1665; found, 361.1672.

(1R,2R,3S,4R,5S)-4-(4-(Phenethylamino)-2-(phenylethynyl)-7H-pyrrolo[2,3-d]pyrimidin-7-yl)bicyclo[3.1.0]hexane-2,3-diol (55). Compound **55** (92%) was prepared from compound **89** by adapting the method provided for compound **54**. ¹H NMR (CD₃OD, 400 MHz): δ 7.70 (d, *J* = 3.6 Hz, 2H), 7.50–7.43 (m, 4H), 7.30–7.27 (m, 4H), 7.23–7.20 (m, 1H), 6.79 (m, 1H), 5.09 (s, 1H), 4.69 (br s, 1H), 3.89 (t, *J* = 7.2 Hz, 2H), 3.78 (d, *J* = 6.4 Hz, 1H), 3.05 (t, *J* = 7.2 Hz, 2H), 2.00–1.96 (m, 1H), 1.63–1.58 (m, 1H), 1.36–1.34 (m, 1H), 0.79–0.73 (m, 1H). HRMS calcd for $C_{28}H_{27}N_4O_2$ ($M + H$)⁺: 451.2134; found, 451.2133.

(1R,2R,3S,4R,5S)-4-(4-((Dicyclopropylmethyl)amino)-2-(phenylethynyl)-7H-pyrrolo[2,3-d]pyrimidin-7-yl)bicyclo[3.1.0]hexane-2,3-diol (56). PdCl₂(PPh₃)₂ (1.68 mg, 0.0024 mmol), CuI (1.0 mg, 0.0012 mmol), phenylacetylene (8 μL, 0.072 mmol), and triethylamine (16 μL, 0.12 mmol) were added to a solution of compound **58** (5.6 mg, 0.012 mmol) in anhydrous dimethylformamide (DMF) (0.6 mL) and stirred at room temperature for overnight. The solvent was evaporated under vacuum, and the residue was purified on flash silica gel column chromatography (hexane/ethyl acetate = 1:1) to give the compound **56** (4 mg, 80%) as a brownish syrup. ¹H NMR (CD₃OD, 400 MHz): δ 7.66–7.63 (m, 2H), 7.44–7.42 (m, 3H), 7.28 (d, *J* = 3.6 Hz, 1H), 6.72 (d, *J* = 3.6 Hz, 1H), 5.03 (s, 1H), 4.65 (t, *J* = 5.6 Hz, 1H), 3.74 (d, *J* = 6.4 Hz, 1H), 3.59 (t, *J* = 7.6 Hz, 1H), 2.00–1.94 (m, 1H), 1.65–1.60 (m, 1H), 1.38–1.35 (m, 1H), 1.21–1.12 (m, 2H), 0.76–0.71 (m, 1H), 0.59–0.54 (m, 2H), 0.47–0.42 (m, 6H). HRMS calcd for $C_{27}H_{29}N_4O_2$ ($M + H$)⁺: 441.2291; found, 441.2290.

(1R,2R,3S,4R,5S)-4-(2-((5-Bromothiophen-2-yl)ethynyl)-4-((dicyclopropylmethyl)amino)-7H-pyrrolo[2,3-d]pyrimidin-7-yl)bicyclo[3.1.0]hexane-2,3-diol (57). Compound **57** (78%) was prepared from compound **58** by adapting the method provided for compound **56**. ¹H NMR (CD₃OD, 400 MHz): δ 7.28 (d, *J* = 3.6 Hz, 1H), 7.25 (d, *J* = 3.6 Hz, 1H), 7.14 (d, *J* = 4.0 Hz, 1H), 7.20 (d, *J* = 3.6 Hz, 1H), 5.01 (s, 1H), 4.68–4.63 (m, 1H), 3.73 (d, *J* = 6.0 Hz, 1H), 3.56 (t, *J* = 8.0 Hz, 1H), 2.01–1.94 (m, 1H), 1.63–1.59 (m, 1H), 1.37–1.34 (m, 1H), 1.20–1.09 (m, 2H), 0.76–0.67 (m, 1H), 0.59–0.54 (m, 2H), 0.45–0.39 (m, 6H). HRMS calcd for $C_{25}H_{26}N_4O_2SBr$ ($M + H$)⁺: 525.0960; found, 525.0953.

(1R,2R,3S,4R,5S)-4-(4-((Dicyclopropylmethyl)amino)-2-iodo-7H-pyrrolo[2,3-d]pyrimidin-7-yl)bicyclo[3.1.0]hexane-2,3-diol (58). Dowex 50 (40 mg) was added to a solution of compound **87** (67 mg, 0.13 mmol) in MeOH (1 mL)–water (1 mL) and heated at 50 °C for 1.5 h. The reaction mixture was filtered and filtrate was evaporated under vacuum. The residue was purified on flash silica gel column chromatography (hexane/ethylacetate = 1:1) to give the compound **58** (38 mg, 63%). ¹H NMR (CD₃OD, 400 MHz): δ 7.05 (d, *J* = 3.6 Hz, 1H), 6.62 (d, *J* = 3.6 Hz, 1H), 4.93 (s, 1H), 4.67 (t, *J* = 5.6 Hz, 1H), 3.72 (d, *J* = 6.4 Hz, 1H), 1.95–1.91 (m, 1H), 1.57–1.52

(m, 1H), 1.31–1.28 (m, 1H), 1.15–1.07 (m, 2H), 0.74–0.68 (m, 1H), 0.58–0.52 (m, 2H), 0.45–0.34 (m, 6H). HRMS calcd for $C_{19}H_{24}N_4O_2I$ ($M + H$)⁺: 467.0944; found, 467.0947.

Ethyl(3aR,3bS,4aS,5R,5aS)-5-(4-chloro-2-iodo-7H-pyrrolo[2,3-d]pyrimidin-7-yl)-2,2-dimethyltetrahydrocyclopropa[3,4]cyclopenta[1,2-d][1,3]dioxole-3b(3aH)-carboxylate (72). Diisopropyl-azodicarboxylate (DIAD) (0.15 mL, 0.76 mmol) was added to a solution of triphenylphosphine (199 mg, 0.76 mmol) and 7-deaza-2-iodo-6-chloro-purine (212 mg, 0.76 mmol) in dry THF (4 mL) at 0 °C and stirred at room temperature for 10 min. A solution of compound 59 (92 mg, 1.0 mmol) in THF (1 mL) was added to the reaction mixture and stirred overnight at room temperature. The solvent was evaporated, and the residue was purified on flash silica gel column chromatography (hexane/ethyl acetate = 5:1) to give the compound 72 (131 mg, 69%) as a colorless foamy solid. ¹H NMR (CD₃OD, 400 MHz): δ 7.46 (d, *J* = 3.6 Hz, 1H), 6.66 (d, *J* = 3.6 Hz, 1H), 5.83 (d, *J* = 6.8 Hz, 1H), 5.0 (s, 1H), 4.83 (d, *J* = 6.8 Hz, 1H), 4.32–4.24 (m, 2H), 2.28–2.24 (m, 1H), 1.68–1.64 (m, 1H), 1.54–1.51 (m, 4H), 1.33 (d, *J* = 7.2 Hz, 3H), 1.2 (s, 3H). HRMS calculated for $C_{18}H_{20}N_3O_4ClI$ ($M + H$)⁺: 504.0187; found, 504.0191.

Ethyl(3aR,3bS,4aS,5R,5aS)-5-(2-iodo-4-(methylamino)-7H-pyrrolo[2,3-d]pyrimidin-7-yl)-2,2-dimethyltetrahydrocyclopropa[3,4]cyclopenta[1,2-d][1,3]dioxole-3b(3aH)-carboxylate (73). Methylamine hydrochloride (164 mg, 2.43 mmol) and triethylamine (0.67 mL, 4.87 mmol) were added to a solution of compound 72 (245 mg, 0.48 mmol) in methanol (5 mL) and stirred at room temperature for overnight. The reaction mixture was evaporated under vacuum, and the residue was purified on flash column chromatography (hexane/ethyl acetate = 1:1) to give the desired product 73 (198 mg, 82%) as a colorless syrup. ¹H NMR (CD₃OD, 400 MHz): δ 6.91 (d, *J* = 3.6 Hz, 1H), 6.49 (d, *J* = 3.6 Hz, 1H), 5.78 (d, *J* = 6.4 Hz, 1H), 4.93 (s, 1H), 4.74 (d, *J* = 6.8 Hz, 1H), 4.30–4.24 (m, 2H), 3.02 (br s, 3H), 2.19–2.14 (m, 1H), 1.64–1.60 (m, 1H), 1.53 (s, 3H), 1.50 (t, *J* = 5.2 Hz, 1H), 1.32 (t, *J* = 7.2 Hz, 3H), 1.28 (s, 3H). HRMS calcd for $C_{19}H_{24}N_4O_4I$ ($M + H$)⁺: 499.0842; found, 499.0844.

Ethyl(3aR,3bS,4aS,5R,5aS)-5-(4-(cyclopropylamino)-2-iodo-7H-pyrrolo[2,3-d]pyrimidin-7-yl)-2,2-dimethyltetrahydrocyclopropa[3,4]cyclopenta[1,2-d][1,3]dioxole-3b(3aH)-carboxylate (74). Compound 74 (85%) was prepared from compound 72 by adapting the method provided for compound 73. ¹H NMR (CD₃OD, 400 MHz): δ 6.94 (d, *J* = 3.6 Hz, 1H), 6.67 (br s, 1H), 5.81 (d, *J* = 7.2 Hz, 1H), 4.76 (d, *J* = 6.0 Hz, 1H), 4.30–4.22 (m, 2H), 2.96–2.91 (m, 1H), 2.19–2.15 (m, 1H), 1.54–1.60 (m, 1H), 1.53 (s, 3H), 1.50 (t, *J* = 5.6 Hz, 1H), 1.32 (t, *J* = 7.2 Hz, 3H), 1.26 (s, 3H), 0.89–0.85 (m, 2H), 0.64–0.63 (m, 2H). HRMS calcd for $C_{21}H_{26}N_4O_4I$ ($M + H$)⁺: 525.0999; found, 525.0994.

Ethyl(3aR,3bS,4aS,5R,5aS)-5-(4-(cyclopropylmethylamino)-2-iodo-7H-pyrrolo[2,3-d]pyrimidin-7-yl)-2,2-dimethyltetrahydrocyclopropa[3,4]cyclopenta[1,2-d][1,3]dioxole-3b(3aH)-carboxylate (75). Compound 75 (83%) was prepared from compound 72 by adapting the method provided for compound 73. ¹H NMR (CD₃OD, 400 MHz): δ 6.89 (d, *J* = 3.6 Hz, 1H), 6.56 (d, *J* = 3.6 Hz, 1H), 5.80 (d, *J* = 6.8 Hz, 1H), 4.74 (d, *J* = 7.2 Hz, 1H), 4.30–4.21 (m, 2H), 3.36–3.34 (m, 2H), 2.18–2.14 (m, 1H), 1.63–1.59 (m, 1H), 1.52 (s, 3H), 1.48 (t, *J* = 5.6 Hz, 1H), 1.30 (t, *J* = 7.2 Hz, 3H), 1.27 (s, 3H), 1.18–1.08 (m, 1H), 0.54–0.50 (m, 2H), 0.32–0.29 (m,

2H). HRMS calcd for $C_{22}H_{28}N_4O_4I$ ($M + H$)⁺: 539.1155; found, 539.1150.

Ethyl(3aR,3bS,4aS,5R,5aS)-5-(2-iodo-4-(phenethylamino)-7H-pyrrolo[2,3-d]pyrimidin-7-yl)-2,2-dimethyltetrahydrocyclopropa[3,4]cyclopenta[1,2-d][1,3]dioxole-3b(3aH)-carboxylate (76). Compound 76 (85%) was prepared from compound 72 by adapting the method provided for compound 73. ¹H NMR (CD₃OD, 400 MHz): δ 7.28–7.27 (m, 4H), 7.21–7.17 (m, 1H), 6.90 (d, *J* = 3.6 Hz, 1H), 6.48 (d, *J* = 3.6 Hz, 1H), 5.81 (d, *J* = 3.6 Hz, 1H), 5.81 (d, *J* = 6.4 Hz, 1H), 4.75 (d, *J* = 7.2 Hz, 1H), 4.31–4.22 (m, 2H), 3.71 (t, *J* = 7.2 Hz, 2H), 2.94 (d, *J* = 7.2 Hz, 2H), 2.19–2.15 (m, 1H), 1.64–1.60 (m, 1H), 1.53 (s, 3H), 1.50 (t, *J* = 5.2 Hz, 1H), 1.33 (t, *J* = 7.2 Hz, 3H), 1.28 (s, 3H). HRMS calcd for $C_{26}H_{30}N_4O_4I$ ($M + H$)⁺: 589.1312; found, 589.1309.

Ethyl(3aR,3bS,4aS,5R,5aS)-5-(2-((5-chlorothiophen-2-yl)ethynyl)-4-(methylamino)-7H-pyrrolo[2,3-d]pyrimidin-7-yl)-2,2-dimethyltetrahydrocyclopropa[3,4]cyclopenta[1,2-d][1,3]dioxole-3b(3aH)-carboxylate (77). PdCl₂(PPh₃)₂ (19.7 mg, 0.02 mmol), CuI (2.6 mg, 0.01 mmol), 2-chloro-5-ethynylthiophene (100 mg, 0.70 mmol), and triethylamine (0.2 mL, 1.4 mmol) were added to a solution of compound 73 (70 mg, 0.14 mmol) in anhydrous DMF (1.5 mL) and stirred at room temperature overnight. The solvent was evaporated under vacuum, and the residue was purified on flash silica gel column chromatography (hexane/ethyl acetate = 2:1) to give the compound 77 (55 mg, 76%) as a yellow syrup. ¹H NMR (CD₃OD, 400 MHz): δ 7.34 (d, *J* = 4.0 Hz, 1H), 7.09 (d, *J* = 3.6 Hz, 1H), 7.01 (d, *J* = 4.0 Hz, 1H), 6.59 (d, *J* = 3.6 Hz, 1H), 5.82 (d, *J* = 6.4 Hz, 1H), 5.04 (s, 1H), 4.71 (d, *J* = 6.4 Hz, 1H), 4.26–4.16 (m, 2H), 3.08 (s, 3H), 2.25–2.20 (m, 1H), 1.71–1.67 (m, 1H), 1.57–1.64 (m, 4H), 1.28 (s, 3H), 1.24 (t, *J* = 7.2 Hz, 3H). HRMS calcd for $C_{25}H_{26}N_4O_4S$ ($M + H$)⁺: 513.1363; found, 513.1362.

Ethyl(3aR,3bS,4aS,5R,5aS)-5-(2-((5-bromothiophen-2-yl)ethynyl)-4-(methylamino)-7H-pyrrolo[2,3-d]pyrimidin-7-yl)-2,2-dimethyltetrahydrocyclopropa[3,4]cyclopenta[1,2-d][1,3]dioxole-3b(3aH)-carboxylate (78). Compound 78 (72%) was prepared from compound 73 by adapting the method provided for compound 77. ¹H NMR (CD₃OD, 400 MHz): δ 7.32 (d, *J* = 4.0 Hz, 1H), 7.14 (d, *J* = 4.0 Hz, 1H), 7.09 (d, *J* = 3.6 Hz, 1H), 6.59 (d, *J* = 3.6 Hz, 1H), 5.82 (d, *J* = 6.4 Hz, 1H), 5.04 (s, 1H), 4.71 (d, *J* = 6.4 Hz, 1H), 4.26–4.18 (m, 2H), 3.08 (s, 3H), 2.25–2.21 (m, 1H), 1.71–1.67 (m, 1H), 1.57–1.54 (m, 4H), 1.28 (s, 3H), 1.24 (t, *J* = 7.2 Hz, 3H). HRMS calcd for $C_{25}H_{26}N_4O_4SBr$ ($M + H$)⁺: 557.0858; found, 557.0853.

Ethyl(3aR,3bS,4aS,5R,5aS)-2,2-dimethyl-5-(4-(methylamino)-2-(phenylethynyl)-7H-pyrrolo[2,3-d]pyrimidin-7-yl)-tetrahydrocyclopropa[3,4]cyclopenta[1,2-d][1,3]dioxole-3b(3aH)-carboxylate (79). Compound 79 (82%) was prepared from compound 73 by adapting the method provided for compound 77. ¹H NMR (CD₃OD, 400 MHz): δ 7.72–7.70 (m, 2H), 7.45–7.43 (m, 3H), 7.08 (d, *J* = 3.6 Hz, 1H), 6.61 (d, *J* = 3.6 Hz, 1H), 5.86 (d, *J* = 7.2 Hz, 1H), 5.07 (s, 1H), 4.74 (d, *J* = 7.2 Hz, 1H), 4.24–4.15 (m, 2H), 3.10 (s, 3H), 2.25–2.21 (m, 1H), 1.71–1.67 (m, 1H), 1.56 (t, *J* = 5.2 Hz, 1H), 1.54 (s, 3H), 1.29 (s, 3H), 1.21 (t, *J* = 7.2 Hz, 3H). HRMS calcd for $C_{27}H_{29}N_4O_4$ ($M + H$)⁺: 473.2189; found, 473.2191.

Ethyl(3aR,3bS,4aS,5R,5aS)-5-(4-(cyclopropylamino)-2-(phenylethynyl)-7H-pyrrolo[2,3-d]pyrimidin-7-yl)-2,2-dimethyltetrahydrocyclopropa[3,4]cyclopenta[1,2-d][1,3]

dioxole-3b(3aH)-carboxylate (80). Compound **80** (84%) was prepared from compound **74** by adapting the method provided for compound **77**. $^1\text{H NMR}$ (CD_3OD , 400 MHz): δ 7.72–7.70 (m, 2H), 7.45–7.43 (m, 3H), 7.11 (d, $J = 3.2$ Hz, 1H), 6.76 (br s, 1H), 5.86 (d, $J = 6.4$ Hz, 1H), 5.07 (s, 1H), 4.75 (d, $J = 7.2$ Hz, 1H), 4.24–4.15 (m, 2H), 3.02–2.96 (m, 1H), 2.25–2.21 (m, 1H), 1.71–1.67 (m, 1H), 1.56 (t, $J = 5.6$ Hz, 1H), 1.54 (s, 3H), 1.29 (s, 3H), 1.21 (t, $J = 7.2$ Hz, 3H), 0.94–0.89 (m, 2H), 0.70–0.66 (m, 2H). HRMS calcd for $\text{C}_{29}\text{H}_{31}\text{N}_4\text{O}_4$ ($\text{M} + \text{H}$) $^+$: 499.2345; found, 499.2341.

Ethyl(3aR,3bS,4aS,5R,5aS)-5-(4-((cyclopropylmethyl)-amino)-2-(phenylethynyl)-7H-pyrrolo[2,3-d]pyrimidin-7-yl)-2,2-dimethyltetrahydrocyclopropa[3,4]cyclopenta[1,2-d][1,3]dioxole-3b(3aH)-carboxylate (81). Compound **81** (82%) was prepared from compound **75** by adapting the method provided for compound **77**. $^1\text{H NMR}$ (CD_3OD , 400 MHz): δ 7.72–7.69 (m, 2H), 7.44–7.42 (m, 3H), 7.07 (d, $J = 3.6$ Hz, 1H), 6.70 (d, $J = 3.6$ Hz, 1H), 5.85 (d, $J = 6.4$ Hz, 1H), 5.08 (s, 1H), 4.74 (d, $J = 7.2$ Hz, 1H), 4.26–4.12 (m, 2H), 3.46 (d, $J = 6.8$ Hz, 2H), 2.25–2.21 (m, 1H), 1.71–1.67 (m, 1H), 1.56 (t, $J = 5.6$ Hz, 1H), 1.54 (s, 3H), 1.28 (m, 4H), 1.22 (d, $J = 7.2$ Hz, 3H), 0.58–0.54 (m, 2H), 0.35–0.31 (m, 2H). HRMS calcd for $\text{C}_{30}\text{H}_{33}\text{N}_4\text{O}_4$ ($\text{M} + \text{H}$) $^+$: 513.2502; found, 513.2507.

Ethyl(3aR,3bS,4aS,5R,5aS)-2,2-dimethyl-5-(4-(phenethylamino)-2-(phenylethynyl)-7H-pyrrolo[2,3-d]pyrimidin-7-yl)-tetrahydrocyclopropa[3,4]cyclopenta[1,2-d][1,3]dioxole-3b(3aH)-carboxylate (82). Compound **82** (83%) was prepared from compound **76** by adapting the method provided for compound **77**. $^1\text{H NMR}$ (CD_3OD , 400 MHz): δ 7.72–7.71 (m, 2H), 7.45–7.43 (m, 4H), 7.30–7.29 (m, 4H), 7.21–7.18 (m, 1H), 7.08 (d, $J = 3.6$ Hz, 1H), 6.61 (d, $J = 3.6$ Hz, 1H), 5.86 (d, $J = 7.2$ Hz, 1H), 5.08 (s, 1H), 4.74 (d, $J = 6.4$ Hz, 1H), 4.22–4.14 (m, 2H), 3.82 (t, $J = 7.2$ Hz, 2H), 3.02 (d, $J = 7.2$ Hz, 2H), 2.26–2.22 (m, 1H), 1.72–1.68 (m, 1H), 1.57 (t, $J = 5.2$ Hz, 1H), 1.54 (s, 3H), 1.29 (s, 3H), 1.22 (t, $J = 7.2$ Hz, 3H). HRMS calcd for $\text{C}_{34}\text{H}_{35}\text{N}_4\text{O}_4$ ($\text{M} + \text{H}$) $^+$: 563.2658; found, 563.2654.

4-Chloro-7-((3aR,3bR,4aS,5R,5aS)-2,2-dimethylhexahydrocyclopropa[3,4]cyclopenta[1,2-d][1,3]dioxol-5-yl)-2-iodo-7H-pyrrolo[2,3-d]pyrimidine (84). DIAD (0.27 mL, 1.4 mmol) was added to a solution of triphenylphosphine (369 mg, 1.4 mmol) and 7-deaza-2-iodo-6-chloro-purine (295 mg, 1.4 mmol) in dry THF (2 mL) at 0 °C and stirred at room temperature for 10 min. A solution of compound **83** (120 mg, 0.7 mmol) in THF (1.5 mL) was added to the reaction mixture and stirred overnight at room temperature. The solvent was evaporated, and the residue was purified on flash silica gel column chromatography (hexane/ethyl acetate = 5:1) to give the compound **84** (206 mg, 68%) as a colorless foamy solid. $^1\text{H NMR}$ (CD_3OD , 400 MHz): δ 7.55 (d, $J = 3.6$ Hz, 1H), 6.66 (d, $J = 3.6$ Hz, 1H), 5.36–5.33 (m, 1H), 5.13 (s, 1H), 4.66 (d, $J = 7.2$ Hz, 1H), 2.09–2.02 (m, 1H), 1.71–1.65 (m, 1H), 1.52 (s, 3H), 1.24 (s, 3H), 0.96–0.88 (m, 2H). HRMS calcd for $\text{C}_{15}\text{H}_{16}\text{N}_3\text{O}_2\text{ClI}$ ($\text{M} + \text{H}$) $^+$: 431.9976; found, 431.9969.

7-((3aR,3bR,4aS,5R,5aS)-2,2-Dimethylhexahydrocyclopropa[3,4]cyclopenta[1,2-d][1,3]dioxol-5-yl)-2-iodo-N-methyl-7H-pyrrolo[2,3-d]pyrimidin-4-amine (85). Methylamine hydrochloride (63 mg, 0.93 mmol) and triethylamine (0.33 mL, 1.8 mmol) were added to a solution of compound **84** (81 mg, 0.18 mmol) in methanol (2 mL) and stirred at room temperature for overnight. The reaction mixture was evaporated under vacuum, and the residue was purified on

flash column chromatography (hexane/ethyl acetate = 2:1) to give the desired product **85** (66 mg, 83%) as a colorless syrup. $^1\text{H NMR}$ (CD_3OD , 400 MHz): δ 7.03 (d, $J = 3.6$ Hz, 1H), 6.53 (s, 1H), 5.30 (t, $J = 6.0$ Hz, 1H), 5.04 (s, 1H), 4.56 (d, $J = 7.2$ Hz, 1H), 3.03 (br s, 3H), 2.03–1.97 (m, 1H), 1.65–1.60 (m, 1H), 1.51 (s, 3H), 1.24 (s, 3H), 0.93–0.84 (m, 2H). HRMS calcd for $\text{C}_{16}\text{H}_{20}\text{N}_4\text{O}_2\text{I}$ ($\text{M} + \text{H}$) $^+$: 427.0631; found, 427.0635.

7-((3aR,3bR,4aS,5R,5aS)-2,2-Dimethylhexahydrocyclopropa[3,4]cyclopenta[1,2-d][1,3]dioxol-5-yl)-2-iodo-N-phenethyl-7H-pyrrolo[2,3-d]pyrimidin-4-amine (86). Compound **86** (80%) was prepared from compound **84** by adapting the method provided for compound **85**. $^1\text{H NMR}$ (CD_3OD , 400 MHz): δ 7.31–7.20 (m, 4H), 7.21–7.19 (m, 1H), 7.02 (d, $J = 3.6$ Hz, 1H), 6.51 (d, $J = 3.6$ Hz, 1H), 5.30 (t, $J = 6.4$ Hz, 1H), 5.05 (s, 1H), 4.55 (d, $J = 7.2$ Hz, 1H), 3.72 (t, $J = 7.2$ Hz, 2H), 2.95 (t, $J = 7.2$ Hz, 2H), 2.03–1.97 (m, 1H), 1.65–1.60 (m, 1H), 1.51 (s, 3H), 1.24 (s, 3H), 0.93–0.84 (m, 2H). HRMS calcd for $\text{C}_{23}\text{H}_{26}\text{N}_4\text{O}_2\text{I}$ ($\text{M} + \text{H}$) $^+$: 517.1101; found, 517.1093.

N-(Dicyclopropylmethyl)-7-((3aR,3bR,4aS,5R,5aS)-2,2-dimethylhexahydrocyclopropa [3,4]cyclopenta[1,2-d][1,3]dioxol-5-yl)-2-iodo-7H-pyrrolo[2,3-d]pyrimidin-4-amine (87). Dicyclopropylmethyl amine hydrochloride (160 mg, 1.05 mmol) and DIPEA (0.37 mL, 2.1 mmol) were added to a solution of compound **84** (93 mg, 0.21 mmol) in 2-propanol (2 mL) and heated at 100 °C for 2 h under microwave condition. The reaction mixture was evaporated under vacuum, and the residue was purified on flash column chromatography (hexane/ethyl acetate = 2:1) to give the desired product **87** (86 mg, 79%) as a colorless syrup. $^1\text{H NMR}$ (CD_3OD , 400 MHz): δ 7.00 (d, $J = 3.6$ Hz, 1H), 6.63 (d, $J = 6.4$ Hz, 1H), 5.03 (t, $J = 3.6$ Hz, 1H), 5.03 (s, 1H), 4.56 (d, $J = 7.2$ Hz, 1H), 2.01–1.97 (m, 1H), 1.64–1.59 (m, 1H), 1.50 (s, 3H), 1.30 (t, $J = 5.2$ Hz, 1H), 1.23 (s, 3H), 1.14–1.06 (m, 1H), 0.92–0.84 (m, 1H), 0.58–0.52 (m, 2H), 0.45–0.35 (m, 6H). HRMS calcd for $\text{C}_{22}\text{H}_{28}\text{N}_4\text{O}_2\text{I}$ ($\text{M} + \text{H}$) $^+$: 507.1257; found, 507.1264.

7-((3aR,3bR,4aS,5R,5aS)-2,2-Dimethylhexahydrocyclopropa[3,4]cyclopenta[1,2-d][1,3]dioxol-5-yl)-N-methyl-2-(phenylethynyl)-7H-pyrrolo[2,3-d]pyrimidin-4-amine (88). $\text{PdCl}_2(\text{PPh}_3)_2$ (9.8 mg, 0.014 mmol), CuI (1.3 mg, 0.07 mmol), phenylethyne (46 μL , 0.42 mmol), and triethylamine (98 μL , 0.7 mmol) were added to a solution of compound **85** (30 mg, 0.07 mmol) in anhydrous DMF (1.2 mL) and stirred at room temperature overnight. The solvent was evaporated under vacuum, and the residue was purified on flash silica gel column chromatography (hexane/ethyl acetate = 3:1) to give the compound **88** (20 mg, 71%) as a brownish syrup. $^1\text{H NMR}$ (CD_3OD , 400 MHz): δ 7.69–7.66 (m, 2H), 7.44–7.42 (m, 4H), 7.24 (d, $J = 3.6$ Hz, 1H), 6.64 (d, $J = 3.6$ Hz, 1H), 5.30–5.25 (m, 2H), 4.54 (d, $J = 7.2$ Hz, 1H), 3.11 (s, 3H), 2.05–2.01 (m, 1H), 1.72–1.67 (m, 1H), 1.52 (s, 3H), 1.24 (s, 3H), 0.99–0.96 (m, 1H), 0.92–0.88 (m, 1H). HRMS calcd for $\text{C}_{24}\text{H}_{25}\text{N}_4\text{O}_2$ ($\text{M} + \text{H}$) $^+$: 401.1978; found, 401.1983.

7-((3aR,3bR,4aS,5R,5aS)-2,2-Dimethylhexahydrocyclopropa[3,4]cyclopenta[1,2-d][1,3]dioxol-5-yl)-N-phenethyl-2-(phenylethynyl)-7H-pyrrolo[2,3-d]pyrimidin-4-amine (89). Compound **89** (74%) was prepared from compound **86** by adapting the method provided for compound **88**. $^1\text{H NMR}$ (CD_3OD , 400 MHz): δ 7.69–7.67 (m, 2H), 7.44–7.42 (m, 3H), 7.30–7.26 (m, 4H), 7.21 (d, $J = 3.6$ Hz, 1H), 7.20–7.19 (m, 1H), 6.64 (d, $J = 3.6$ Hz, 1H), 5.30–5.26 (m, 2H), 4.54 (d, $J = 7.2$ Hz, 1H), 3.83 (t, $J = 7.2$ Hz, 2H),

3.03–2.99 (t, $J = 7.2$ Hz, 2H), 2.06–2.01 (m, 1H), 1.72–1.67 (m, 1H), 1.52 (s, 3H), 1.24 (s, 3H), 1.00–0.96 (m, 1H), 0.92–0.87 (m, 1H). HRMS calcd for $C_{31}H_{31}N_4O_2$ ($M + H$)⁺: 491.2447; found, 491.2449.

N-(Dicyclopropylmethyl)-7-((3*aR*,3*bR*,4*aS*,5*R*,5*aS*)-2,2-dimethylhexahydrocyclopropa[3,4]cyclopenta[1,2-*d*][1,3]-dioxol-5-yl)-2-(phenylethynyl)-7*H*-pyrrolo[2,3-*d*]pyrimidin-4-amine (**90**). Compound **90** (73%) was prepared from compound **87** by adapting the method provided for compound **88**. ¹H NMR (CD₃OD, 400 MHz): δ 7.65–7.66 (m, 2H), 7.43–7.42 (m, 3H), 7.23 (d, $J = 3.6$ Hz, 1H), 6.76 (d, $J = 3.6$ Hz, 1H), 5.30–5.25 (m, 2H), 4.54 (d, $J = 7.2$ Hz, 1H), 3.59 (t, $J = 3.6$ Hz, 1H), 2.07–2.01 (m, 1H), 1.73–1.68 (m, 1H), 1.52 (s, 3H), 1.24 (s, 3H), 1.21–1.12 (m, 2H), 1.00–0.97 (m, 1H), 0.92–0.87 (m, 1H), 0.59–0.54 (m, 2H), 0.46–0.41 (m, 6H). HRMS calcd for $C_{30}H_{33}N_4O_2$ ($M + H$)⁺: 481.2604; found, 481.2609.

2-((5-Bromothiophen-2-yl)ethynyl)-*N*-(dicyclopropylmethyl)-7-((3*aR*,3*bR*,4*aS*,5*R*,5*aS*)-2,2-dimethylhexahydrocyclopropa[3,4]cyclopenta[1,2-*d*][1,3]-dioxol-5-yl)-7*H*-pyrrolo[2,3-*d*]pyrimidin-4-amine (**91**). Compound **91** (71%) was prepared from compound **87** by adapting the method provided for compound **88**. ¹H NMR (CD₃OD, 400 MHz): δ 7.26 (d, $J = 4.0$ Hz, 1H), 7.24 (d, $J = 3.6$ Hz, 1H), 7.13 (d, $J = 4.0$ Hz, 1H), 6.75 (d, $J = 3.6$ Hz, 1H), 5.29 (t, $J = 6.0$ Hz, 1H), 5.22 (s, 1H), 4.53 (d, $J = 7.2$ Hz, 1H), 3.58 (t, $J = 8.0$ Hz, 1H), 2.06–2.00 (m, 1H), 1.72–1.67 (m, 1H), 1.52 (s, 3H), 1.30 (t, $J = 5.2$ Hz, 1H), 1.24 (s, 3H), 1.20–1.11 (m, 1H), 0.99–0.95 (m, 1H), 0.92–0.86 (m, 1H), 0.58–0.53 (m, 2H), 0.45–0.39 (m, 6H). HRMS calcd for $C_{28}H_{30}N_4O_2SBr$ ($M + H$)⁺: 565.1095; found, 565.1089.

Pharmacological Procedures. Radioligand Binding and Uptake Assays. Initial screening at ORs and other drug targets was performed by the PDSP. K_i determinations using 96-well plates and binding profiles in a broad screen of receptors and channels were generously provided by the National Institute of Mental Health's Psychoactive Drug Screening Program, Contract # HHSN-271-2008-00025-C (NIMH PDSP). The NIMH PDSP is directed by Bryan L. Roth MD, PhD at the University of North Carolina at Chapel Hill and Project Officer Jamie Driscoll at NIMH, Bethesda MD, USA. For experimental details please refer to the PDSP web site at: <https://pdspdb.unc.edu/pdspWeb/content/PDSP%20Protocols%20II%202013-03-28.pdf>. The cell line used for preparing membranes for binding in human KOR, DOR, and MOR is HEK-293s cells stably expressing the receptors, grown in DMEM medium containing 200 (DOR and MOR) or 500 (KOR) μ g/mL geneticin, 10% fetal bovine serum, and penicillin/streptomycin (1 U/mL). The buffer used for binding was 50 mM Tris-HCl, 10 mM MgCl₂, 0.1 mM EDTA, pH 7.4, room temperature. The buffer used for washing was 50 mM Tris-HCl, pH 7.4, 4° to 8 °C. The radioligand K_d values (and concentration range used, nM) were [³H]Tyr-D-Ala-Gly-Phe-D-Leu ([³H]DADLE, **97**) for DOR, 1.85 ± 0.15 (1.0–2.0) nM; [³H]*N*-methyl-2-phenyl-*N*-[(5*R*,7*S*,8*S*)-7-(pyrrolidin-1-yl)-1-oxaspiro[4.5]dec-8-yl]acetamide ([³H]U69593, **98**) for KOR, 1.07 ± 0.10 (0.6–1.2) nM; and [³H]Ala²-MePhe⁴-Glyol⁵-Enkephalin ([³H]DAMGO, **99**) for MOR, 1.73 ± 0.14 (1.0–2.0) nM. The hDOR, hKOR, and hMOR reference ligands had K_i values of natrindole **108**, 0.81 ± 0.08 nM; salvinorin A **109**, 1.93 ± 0.45 nM; and morphine **110**, 2.62 ± 0.22 nM, respectively.

The radioligand for binding in membranes of HEKT cells expressing hNOP was [³H]nociceptin **100** (pK_i 9.11 ± 0.12 , 0.5 – 2.0 nM used), and the reference ligand was 7-[[4-(2,6-dichlorophenyl)-1-piperidinyl]methyl]-6,7,8,9-tetrahydro-1-methyl-5*H*-benzocyclohepten-5-ol (SB612111), **111** ($K_i = 6.58 \pm 1.42$ nM).

The buffer used for TSPO binding was 50 mM Tris-acetate, pH 7.4, room temperature. The reference ligand 4'-chlorodiazepam for TSPO binding had a K_i value of 27.6 ± 2.3 nM.

Binding assays at DAT, NET, and SERT were performed as described.^{5,8,40} The protein content and K_i values were determined, as reported.^{50,51} The radioligands used by PDSP for NET and SERT binding were [³H](*R,S*)-3-(2-methoxyphenoxy)-*N*-methyl-3-phenylpropan-1-amine **104** and [³H](*R,S*)-1-[3-(dimethylamino)propyl]-1-(4-fluorophenyl)-1,3-dihydroisobenzofuran-5-carbonitrile **105**, respectively.

β Arrestin2 Recruitment Assay. The DiscoveRx PathHunter enzyme complementation assay (PathHunter U2OS OPRK1 β -Arrestin Cell Line) cell line was used to assess β arrestin2 recruitment to KOR according to the manufacturer's instruction and as described in detail previously.⁵³ Nonlinear regression analysis was used to generate I_{MAX} , EC_{50} and IC_{50} values in GraphPad Prism, v. 7.0 (San Diego, CA).

cAMP Accumulation Assay. Cyclic AMP accumulation was measured by treating CHO cells stably expressing the hKOR with test compounds in the presence of 20 μ M forskolin and 25 μ M 4-(3-butoxy-4-methoxybenzyl)imidazolidin-2-one for 30 min at room temperature. Detection of cAMP accumulation was done using Cisbio's dynamic 2 kit (Cisbio Bioassays, Bedford, MA) according to the manufacturer's instructions. Data were analyzed using GraphPad Prism, v. 7.0 (San Diego, CA).

■ ASSOCIATED CONTENT

Supporting Information

The Supporting Information is available free of charge on the ACS Publications website at DOI: [10.1021/acsomega.8b01237](https://doi.org/10.1021/acsomega.8b01237).

PDB file of the following ligand–protein complex: minimized lowest IE structure returned during the MD simulation of **28** in the hKOR HSE model (PDB)

PDB file of the following ligand–protein complex: minimized lowest IE structure returned during the MD simulation of **28** in the hKOR HSD model (complexes superimposed in Figure 5C) (PDB)

MD simulation of **28** (Video S1) (AVI)

Chemical strings file (CSV).

Chemical synthesis (with Schemes S1–S4); reagents for diverse and off-target binding activities; binding inhibition curves (KOR and TSPO, Figures S1–S4); binding inhibition curves (other off-targets, Figure S5); parameters for interaction with DAT and NET (Table S1); lack of correlation of binding at KOR and TSPO (Figure S6); molecular modeling procedures and results (Table S2 and Figure S7); and pharmacokinetic methods and ADME-toxicity data for **28** (Tables S3–S7 and Figures 8 and 9) (PDF)

AUTHOR INFORMATION

Corresponding Author

*E-mail: kennethj@niddk.nih.gov. Phone: 301-496-9024. Fax: 301-496-8422 (K.A.J.).

ORCID

Antonella Ciancetta: [0000-0002-7612-2050](https://orcid.org/0000-0002-7612-2050)

Kenneth A. Jacobson: [0000-0001-8104-1493](https://orcid.org/0000-0001-8104-1493)

Present Address

[#]Queen's University Belfast, School of Pharmacy, 96 Lisburn Rd, Belfast BT9 7BL, UK.

Author Contributions

[†]D.K.T. and A.C. contributed equally.

Notes

The authors declare no competing financial interest.

ACKNOWLEDGMENTS

We acknowledge the support from the NIH Intramural Research Program (NIDDK, ZIA DK031117-28). We thank John Lloyd (NIDDK) for mass spectral determinations and Robert O'Connor (NIDDK) for NMR spectra. We thank Dr. Bryan L. Roth (University of North Carolina at Chapel Hill) and National Institute of Mental Health's Psychoactive Drug Screening Program (contract # HHSN-271-2008-00025-C) for screening data. We also thank the NIH National Institute on Drug Abuse (NIDA)/VA Interagency Agreement #ADA12013; the Methamphetamine Abuse Research Center (P50 DA018165-06), and the Department of Veterans Affairs Research Career Scientist and Merit Review Programs, and NIDA (R01DA031297) to L.M.B.

ABBREVIATIONS

AR, adenosine receptor; HEK 293, human embryonic kidney 293; DAT, the dopamine transporter; DMF, dimethylformamide; DIAD, diisopropyl-azodicarboxylate; DIPEA, diisopropylethylamine; DOR, δ -opioid receptor; GPCR, G protein-coupled receptor; HRMS, high resolution mass spectrometry; HSD, His protonated on the N ^{δ} atom; HSE, His protonated on the N ^{ϵ} atom; IE, interaction energy; IFD, Induced Fit Docking; KOR, κ -opioid receptor; MD, molecular dynamics; MOR, μ -opioid receptor; NET, the norepinephrine transporter; NOP, nociceptin receptor; PDSP, Psychoactive Drug Screening Program; RMSD, root mean square deviation; SAR, structure–activity relationship; SERT, the serotonin transporter; Tango, transcriptional activation following arrestin translocation; TBAP, tetrabutylammonium dihydrogenphosphate; TFA, trifluoroacetic acid; THF, Tetrahydrofuran; TIPSCl, tri-isopropylsilyl chloride; TM, transmembrane; TSPO, the translocator protein.

REFERENCES

- (1) Little, J. W.; Ford, A.; Symons-Liguori, A. M.; Chen, Z.; Janes, K.; Doyle, T.; Xie, J.; Luongo, L.; Tosh, D. K.; Maione, S.; Bannister, K.; Dickenson, A. H.; Vanderah, T. W.; Porreca, F.; Jacobson, K. A.; Salvemini, D. Endogenous adenosine A3 receptor activation selectively alleviates persistent pain states. *Brain* **2015**, *138*, 28–35.
- (2) Tosh, D. K.; Finley, A.; Paoletta, S.; Moss, S. M.; Gao, Z.-G.; Gizewski, E. T.; Auchampach, J. A.; Salvemini, D.; Jacobson, K. A. In Vivo Phenotypic Screening for Treating Chronic Neuropathic Pain: Modification of C2-Arylethynyl Group of Conformationally Constrained A3 Adenosine Receptor Agonists. *J. Med. Chem.* **2014**, *57*, 9901–9914.

- (3) Tosh, D. K.; Deflorian, F.; Phan, K.; Gao, Z.-G.; Wan, T. C.; Gizewski, E.; Auchampach, J. A.; Jacobson, K. A. Structure-Guided Design of A3 Adenosine Receptor-Selective Nucleosides: Combination of 2-Arylethynyl and Bicyclo[3.1.0]hexane Substitutions. *J. Med. Chem.* **2012**, *55*, 4847–4860.

- (4) Jacobson, K. A.; Tosh, D. K.; Toti, K. S.; Ciancetta, A. Polypharmacology of conformationally locked methanocarb nucleosides. *Drug Discovery Today* **2017**, *22*, 1782–1791.

- (5) Tosh, D. K.; Ciancetta, A.; Warnick, E.; Crane, S.; Gao, Z.-G.; Jacobson, K. A. Structure-Based Scaffold Repurposing for G Protein-Coupled Receptors: Transformation of Adenosine Derivatives into 5HT2B/5HT2C Serotonin Receptor Antagonists. *J. Med. Chem.* **2016**, *59*, 11006–11026.

- (6) Tosh, D. K.; Janowsky, A.; Eshleman, A. J.; Warnick, E.; Gao, Z.-G.; Chen, Z.; Gizewski, E.; Auchampach, J. A.; Salvemini, D.; Jacobson, K. A. Scaffold repurposing of nucleosides (adenosine receptor agonists): enhanced activity at the human dopamine and norepinephrine sodium symporters. *J. Med. Chem.* **2017**, *60*, 3109–3123.

- (7) De Coen, L. M.; Heugebaert, T. S. A.; García, D.; Stevens, C. V. Synthetic entries to and biological activity of pyrrolopyrimidines. *Chem. Rev.* **2016**, *116*, 80–139.

- (8) Perliková, P.; Hocek, M. Pyrrolo[2,3-d]pyrimidine (7-deazapurine) as a privileged scaffold in design of antitumor and antiviral nucleosides. *Med. Res. Rev.* **2017**, *37*, 1429–1460.

- (9) Goldfeld, D. A.; Murphy, R.; Kim, B.; Wang, L.; Beuming, T.; Abel, R.; Friesner, R. A. Docking and free energy perturbation studies of ligand binding in the kappa opioid receptor. *J. Phys. Chem. B* **2015**, *119*, 824–835.

- (10) Zheng, Z.; Huang, X.-P.; Mangano, T. J.; Zou, R.; Chen, X.; Zaidi, S. A.; Roth, B. L.; Stevens, R. C.; Katritch, V. Structure-Based Discovery of New Antagonist and Biased Agonist Chemotypes for the Kappa Opioid Receptor. *J. Med. Chem.* **2017**, *60*, 3070–3081.

- (11) Marino, K. A.; Shang, Y.; Filizola, M. Insights into the function of opioid receptors from molecular dynamics simulations of available crystal structures. *Br. J. Pharmacol.* **2017**, *175*, 2834–2845.

- (12) Stevens, W. C.; Jones, R. M.; Subramanian, G.; Metzger, T. G.; Ferguson, D. M.; Portoghese, P. S. Potent and selective indolomorphinan antagonists of the kappa-opioid receptor. *J. Med. Chem.* **2000**, *43*, 2759–2769.

- (13) Thomas, J. B.; Atkinson, R. N.; Vinson, N. A.; Catanzaro, J. L.; Perretta, C. L.; Fix, S. E.; Mascarella, S. W.; Rothman, R. B.; Xu, H.; Dersch, C. M.; Cantrell, B. E.; Zimmerman, D. M.; Carroll, F. I. Identification of (3R)-7-Hydroxy-N-((1S)-1-[(3R,4R)-4-(3-hydroxyphenyl)-3,4-dimethyl-1-piperidinyl]methyl]-2-methylpropyl)-1,2,3,4-tetrahydro-3-isoquinolinecarboxamide as a Novel Potent and Selective Opioid κ Receptor Antagonist. *J. Med. Chem.* **2003**, *46*, 3127–3137.

- (14) Urbano, M.; Guerrero, M.; Rosen, H.; Roberts, E. Antagonists of the kappa opioid receptor. *Bioorg. Med. Chem. Lett.* **2014**, *24*, 2021–2032.

- (15) Rorick-Kehn, L. M.; Witkin, J. M.; Statnick, M. A.; Eberle, E. L.; McKinzie, J. H.; Kahl, S. D.; Forster, B. M.; Wong, C. J.; Li, X.; Crile, R. S.; Shaw, D. B.; Sahr, A. E.; Adams, B. L.; Quimby, S. J.; Diaz, N.; Jimenez, A.; Pedregal, C.; Mitch, C. H.; Knopp, K. L.; Anderson, W. H.; Cramer, J. W.; McKinzie, D. L. LY2456302 is a novel, potent, orally-bioavailable small molecule kappa-selective antagonist with activity in animal models predictive of efficacy in mood and addictive disorders. *Neuropharmacology* **2014**, *77*, 131–144.

- (16) Dale, E.; Bang-Andersen, B.; Sánchez, C. Emerging mechanisms and treatments for depression beyond SSRIs and SNRIs. *Biochem. Pharmacol.* **2015**, *95*, 81–97.

- (17) Carroll, F. I.; Carlezon, W. A. Development of κ Opioid Receptor Antagonists. *J. Med. Chem.* **2013**, *56*, 2178–2195.

- (18) Crowley, N. A.; Bloodgood, D. W.; Hardaway, J. A.; Kendra, A. M.; McCall, J. G.; Al-Hasani, R.; McCall, N. M.; Yu, W.; Schools, Z. L.; Krashes, M. J.; Lowell, B. B.; Whistler, J. L.; Bruchas, M. R.; Kash, T. L. Dynorphin controls the gain of an amygdalar anxiety circuit. *Cell Rep.* **2016**, *14*, 2774–2783.

- (19) Kuzumaki, N.; Suzuki, A.; Narita, M.; Hosoya, T.; Nagasawa, A.; Imai, S.; Yamamizu, K.; Morita, H.; Nagase, H.; Okada, Y.; Okano, H. J.; Yamashita, J. K.; Okano, H.; Suzuki, T.; Narita, M. Effect of κ -opioid receptor agonist on the growth of non-small cell lung cancer (NSCLC) cells. *Br. J. Cancer* **2012**, *106*, 1148–1152.
- (20) Turnaturi, R.; Aricò, G.; Ronsisvalle, G.; Parenti, C.; Pasquinucci, L. Multitarget opioid ligands in pain relief: New players in an old game. *Eur. J. Med. Chem.* **2016**, *108*, 211–228.
- (21) Leppert, W. Emerging therapies for patients with symptoms of opioid-induced bowel dysfunction. *Drug Des., Dev. Ther.* **2015**, *2015*, 2215–2231.
- (22) (a) Holzer, P. Non-analgesic effects of opioids: Management of opioid-induced constipation by peripheral opioid receptor antagonists: Prevention or withdrawal? *Curr. Pharm. Des.* **2012**, *18*, 6010–6020. (b) Anantharamu, T.; Sharma, S.; Gupta, A.; Dahiya, N.; Singh Brashier, D.; Sharma, A. Naloxegol: First oral peripherally acting mu opioid receptor antagonists for opioid-induced constipation. *J. Pharmacol. Pharmacother.* **2015**, *6*, 188–192.
- (23) Da Pozzo, E.; Giacomelli, C.; Costa, B.; Cavallini, C.; Taliani, S.; Barresi, E.; Da Settimo, F.; Martini, C. TSPO PIGA ligands promote neurosteroidogenesis and human astrocyte well-being. *Int. J. Mol. Sci.* **2016**, *17*, 1028.
- (24) Costa, B.; Da Pozzo, E.; Giacomelli, C.; Barresi, E.; Taliani, S.; Da Settimo, F.; Martini, C. TSPO ligand residence time: a new parameter to predict compound neurosteroidogenic efficacy. *Sci. Rep.* **2016**, *6*, 18164.
- (25) Barresi, E.; Bruno, A.; Taliani, S.; Cosconati, S.; Da Pozzo, E.; Salerno, S.; Simorini, F.; Daniele, S.; Giacomelli, C.; Marini, A. M.; La Motta, C.; Marinelli, L.; Cosimelli, B.; Novellino, E.; Greco, G.; Da Settimo, F.; Martini, C. Deepening the topology of the translocator protein binding site by novel N,N-dialkyl-2-arylindol-3-ylglyoxylamides. *J. Med. Chem.* **2015**, *58*, 6081–6092.
- (26) Lenglet, T.; Lacomblez, L.; Abitbol, J. L.; Ludolph, A.; Mora, J. S.; Robberecht, W.; Shaw, P. J.; Pruss, R. M.; Cuvier, V.; Meininger, V. A phase II–III trial of olesoxime in subjects with amyotrophic lateral sclerosis. *Eur. J. Neurol.* **2014**, *21*, 529–536.
- (27) Daniele, S.; Barresi, E.; Zappelli, E.; Marinelli, L.; Novellino, E.; Da Settimo, F.; Taliani, S.; Trincavelli, M. L.; Martini, C. Long lasting MDM2/Translocator protein modulator: a new strategy for irreversible apoptosis of human glioblastoma cells. *Oncotarget* **2016**, *7*, 7866–7884.
- (28) Damont, A.; Médran-Navarrete, V.; Cacheux, F.; Kuhnast, B.; Pottier, G.; Bernards, N.; Marguet, F.; Puech, F.; Boisgard, R.; Dollé, F. Novel Pyrazolo[1,5-a]pyrimidines as Translocator Protein 18 kDa (TSPO) Ligands: Synthesis, in Vitro Biological Evaluation, [18F]-Labeling, and in Vivo Neuroinflammation PET Images. *J. Med. Chem.* **2015**, *58*, 7449–7464.
- (29) Li, F.; Liu, J.; Liu, N.; Kuhn, L. A.; Garavito, R. M.; Ferguson-Miller, S. Translocator protein 18 kDa (TSPO): An old protein with new functions? *Biochemistry* **2016**, *55*, 2821–2831.
- (30) Gavish, M.; Bachman, I.; Shoukrun, R.; Katz, Y.; Veenman, L.; Weisinger, G.; Weizman, A. Enigma of the peripheral benzodiazepine receptor. *Pharmacol. Rev.* **1999**, *51*, 629–650.
- (31) Daugherty, D. J.; Selvaraj, V.; Chechneva, O. V.; Liu, X.-B.; Pleasure, D. E.; Deng, W. A TSPO ligand is protective in a mouse model of multiple sclerosis. *EMBO Mol. Med.* **2013**, *5*, 891–903.
- (32) Maruoka, H.; Barrett, M. O.; Ko, H.; Tosh, D. K.; Melman, A.; Burianek, L. E.; Balasubramanian, R.; Berk, B.; Costanzi, S.; Harden, T. K.; Jacobson, K. A. Pyrimidine Ribonucleotides with Enhanced Selectivity as P2Y6 Receptor Agonists: Novel 4-Alkylxyimino, (S)-Methanocarpa, and 5'-Triphosphate γ -Ester Modifications[†]. *J. Med. Chem.* **2010**, *53*, 4488–4501.
- (33) Paoletta, S.; Tosh, D. K.; Finley, A.; Gizewski, E. T.; Moss, S. M.; Gao, Z.-G.; Auchampach, J. A.; Salvemini, D.; Jacobson, K. A. Rational Design of Sulfonated A3 Adenosine Receptor-Selective Nucleosides as Pharmacological Tools To Study Chronic Neuropathic Pain. *J. Med. Chem.* **2013**, *56*, 5949–5963.
- (34) Tosh, D. K.; Paoletta, S.; Chen, Z.; Moss, S. M.; Gao, Z.-G.; Salvemini, D.; Jacobson, K. A. Extended N⁶ substitution of rigid C2-arylethynyl nucleosides for exploring the role of extracellular loops in ligand recognition at the A3 adenosine receptor. *Bioorg. Med. Chem. Lett.* **2014**, *24*, 3302–3306.
- (35) Tosh, D. K.; Paoletta, S.; Phan, K.; Gao, Z.-G.; Jacobson, K. A. Truncated Nucleosides as A3 Adenosine Receptor Ligands: Combined 2-Arylethynyl and Bicyclohexane Substitutions. *ACS Med. Chem. Lett.* **2012**, *3*, 596–601.
- (36) Tosh, D. K.; Padia, J.; Salvemini, D.; Jacobson, K. A. Efficient, large-scale synthesis and preclinical studies of MRS5698, a highly selective A3 adenosine receptor agonist that protects against chronic neuropathic pain. *Purinergic Signalling* **2015**, *11*, 371–387.
- (37) Tosh, D. K.; Crane, S.; Chen, Z.; Paoletta, S.; Gao, Z.-G.; Gizewski, E.; Auchampach, J. A.; Salvemini, D.; Jacobson, K. A. Rigidified A3 Adenosine Receptor Agonists: 1-Deazaadenine Modification Maintains High in Vivo Efficacy. *ACS Med. Chem. Lett.* **2015**, *6*, 804–808.
- (38) Joshi, B. V.; Melman, A.; Mackman, R. L.; Jacobson, K. A. Synthesis of ethyl (1S,2R,3S,4S,5S)-2,3-O-(isopropylidene)-4-hydroxy-bicyclo[3.1.0]hexane-carboxylate from L-ribose: A versatile chiral synthon for preparation of adenosine and P2 receptor ligands. *Nucleosides, Nucleotides Nucleic Acids* **2008**, *27*, 279–291.
- (39) Tosh, D. K.; Chinn, M.; Ivanov, A. A.; Klutz, A. M.; Gao, Z.-G.; Jacobson, K. A. Functionalized Congeners of A3 Adenosine Receptor-Selective Nucleosides Containing a Bicyclo[3.1.0]hexane Ring System[†]. *J. Med. Chem.* **2009**, *52*, 7580–7592.
- (40) Besnard, J.; Ruda, G. F.; Setola, V.; Abecassis, K.; Rodriguiz, R. M.; Huang, X.-P.; Norval, S.; Sassano, M. F.; Shin, A. I.; Webster, L. A.; Simeons, F. R. C.; Stojanovski, L.; Prat, A.; Seidah, N. G.; Constam, D. B.; Bickerton, G. R.; Read, K. D.; Wetsel, W. C.; Gilbert, I. H.; Roth, B. L.; Hopkins, A. L. Automated design of ligands to polypharmacological profiles. *Nature* **2012**, *492*, 215–220.
- (41) Zaveri, N. T. Nociceptin opioid receptor (NOP) as a therapeutic target: progress in translation from preclinical research to clinical utility. *J. Med. Chem.* **2016**, *59*, 7011–7028.
- (42) Kroeze, W. K.; Sassano, M. F.; Huang, X.-P.; Lansu, K.; McCorvy, J. D.; Giguère, P. M.; Sciaky, N.; Roth, B. L. PRESTO-Tango as an open-source resource for interrogation of the druggable human GPCRome. *Nat. Struct. Mol. Biol.* **2015**, *22*, 362–369.
- (43) Wu, H.; Wacker, D.; Mileni, M.; Katritch, V.; Han, G. W.; Vardy, E.; Liu, W.; Thompson, A. A.; Huang, X.-P.; Carroll, F. I.; Mascarella, S. W.; Westkaemper, R. B.; Mosier, P. D.; Roth, B. L.; Cherezov, V.; Stevens, R. C. Structure of the human κ -opioid receptor in complex with JDTic. *Nature* **2012**, *485*, 327–332.
- (44) Manglik, A.; Kruse, A. C.; Kobilka, T. S.; Thian, F. S.; Mathiesen, J. M.; Sunahara, R. K.; Pardo, L.; Weis, W. I.; Kobilka, B. K.; Granier, S. Crystal structure of the μ -opioid receptor bound to a morphinan antagonist. *Nature* **2012**, *485*, 321–326.
- (45) Granier, S.; Manglik, A.; Kruse, A. C.; Kobilka, T. S.; Thian, F. S.; Weis, W. I.; Kobilka, B. K. Structure of the δ -opioid receptor bound to naltrindole. *Nature* **2012**, *485*, 400–404.
- (46) Van't Veer, A.; Carlezon, W. A., Jr. Role of kappa-opioid receptors in stress and anxiety-related behavior. *Psychopharmacology* **2013**, *229*, 435–452.
- (47) Schaddelee, M. P.; Read, K. D.; Cleypool, C. G. J.; IJzerman, A. P.; Danhof, M.; de Boer, A. G. Brain penetration of synthetic adenosine A1 receptor agonists in situ: role of the rENT1 nucleoside transporter and binding to blood constituents. *Eur. J. Pharm. Sci.* **2005**, *24*, 59–66.
- (48) (a) Mathew, B.; Lennon, F. E.; Siegler, J.; Mirzapoiazova, T.; Mambetsariev, N.; Sammani, S.; Gerhold, L. M.; LaRivière, P. J.; Chen, C.-T.; Garcia, J. G. N.; Salgia, R.; Moss, J.; Singleton, P. A. The Novel Role of the Mu Opioid Receptor in Lung Cancer Progression. *Anesth. Analg.* **2011**, *112*, 558–567. (b) Janku, F.; Johnson, L. K.; Karp, D. D.; Atkins, J. T.; Singleton, P. A.; Moss, J. Treatment with methyl naltrexone is associated with increased survival in patients with advanced cancer. *Ann. Oncol.* **2016**, *27*, 2032–2038.
- (49) Sadowski, I.; Ma, J.; Triezenberg, S.; Ptashne, M. GAL4-VP16 is an unusually potent transcriptional activator. *Nature* **1988**, *335*, 563–564.

(50) Yung-Chi, C.; Prusoff, W. H. Relationship between inhibition constant (K_I) and concentration of inhibitor which causes 50 percent inhibition (I_{50}) of an enzymatic-reaction. *Biochem. Pharmacol.* **1973**, *22*, 3099–3108.

(51) Bradford, M. M. A rapid and sensitive method for the quantitation of microgram quantities of protein utilizing the principle of protein-dye binding. *Anal. Biochem.* **1976**, *72*, 248–254.

(52) Li, F.; Liu, J.; Zheng, Y.; Garavito, R. M.; Ferguson-Miller, S. Crystal structures of translocator protein (TSPO) and mutant mimic of a human polymorphism. *Science* **2015**, *347*, 555–558.

(53) Zhou, L.; Lovell, K. M.; Frankowski, K. J.; Slauson, S. R.; Phillips, A. M.; Streicher, J. M.; Stahl, E.; Schmid, C. L.; Hodder, P.; Madoux, F.; Cameron, M. D.; Prisinzano, T. E.; Aubé, J.; Bohn, L. M. Development of functionally selective, small molecule agonists at kappa opioid receptors. *J. Biol. Chem.* **2013**, *288*, 36703–36716.